AD706024

URS RESEARCH COMPANY

A URS Systems Affiliate

02

URS 679-6

HYDRODYNAMIC DATA FROM EXPLODING WIRES

April 1, 1970

Annual Report

by

A. R. Kriebel
J. S. Bechtel

URS RESEARCH COMPANY
155 Bovet Road
San Mateo, California 94402

for

OFFICE OF NAVAL RESEARCH
Department of the Navy
Washington, D.C. 20360

Contract No. ~~N0014-~~67-C-0451
N00014-

CONTENTS

NOMENCLATURE

A_{max}	Maximum bubble radius = $D_{max}/2$ (in. or ft as indicated)
d	Depth of burst (in. or ft as indicated)
d_w	Water depth (in. or ft as indicated)
D	Charge diameter (in.)
D_{max}	Maximum bubble diameter = $2A_{max}$ (in. of ft as indicated)
F	Function of σ
g	Acceleration of gravity (32.2 ft/sec^2)
G	Function of cavity shape and σ
K	Ratio of measured to calculated peak wave height
P_a	Atmospheric pressure (psia or atm)
P_m	Peak pressure of underwater shock wave (psi)
r	Slant range (ft)
R	Horizontal range from charge (in. or ft as indicated)
R_c	Cavity radius at waterline, when cavity depth is maximum (in.)
R_o	Radius of equivalent TNT charge, $\simeq$0.072 in.
t	Time from release of cavity (sec)
t_c	Time from detonation to formation of maximum cavity depth (sec)
t_m	Time from detonation to arrival of peak wave (sec)
W	Equivalent TNT charge weight for exploding wire (gm or lb), $\simeq$0.038 gm
W_N	Equivalent nuclear yield for exploding wire (gm or lb), $\simeq$0.045 gm
Z	Hydrostatic and atmospheric heads, d(ft)+34
T	Time shift for matching calculated and measured peak wave (sec)
λ	Wavelength (ft)
η_m	Peak wave height above waterline (in. or ft as indicated)
σ	An independent variable defined by Eq. (13)
τ	Wave period (sec)

Section 1
INTRODUCTION

A series of experiments with exploding wires was conducted recently at the Shock Hydrodynamic Facility of Engineering-Physics Company (EPCO) under ONR sponsorship (Ref. 1). The purpose was to obtain hydrodynamic data in the proximity of explosions occurring near the surface of deep water. Data illustrating the phenomenon of the "upper critical depth" for the generation of water surface waves was one primary objective. The experimental results are particularly interesting since no nuclear bursts have been fired under similar test conditions, i.e., near the surface of deep water.

Forty-one nearly identical wires were exploded at distances between 4 in. above to 4 in. below the surface of a large volume of water under normal atmospheric pressure. The horizontal diameter of the expanded bubbles and cavities was nearly constant and equal to 4 in. for the submerged shots, as shown by Fig. 4. The equivalent "nuclear" yield was 0.045 gm, (or 0.038 gm of TNT) based on the bubble radius for the deepest shot. The data will be reported here and compared with previous exploding wire data (Ref. 2); unclassified full-scale nuclear data (at the same scaled depth of burst in shallow water, i.e., shot CROSSROADS-Baker); data from large HE charges (Refs. 3 and 4); and data from three small HE charges with yields equivalent to 0.054, 0.17, and 1.57 gm of TNT (Ref. 5).

The cavity data were obtained at EPCO with a Schlieren optical system and a framing camera which provided 1-μsec exposures at 40-μsec intervals on 35-mm film strips. Sample prints are shown in Fig. 3 for the five shots indicated in Fig. 4.

The water shock waves were measured with three crystal pressure transducers (Atlantic Research LC series). The three gages were located at a horizontal range of 6 in., and at depths of 1, 6, and 21 in. Sample pressure-time histories are shown in Fig. 5.

Water surface waves were measured photographically at a range of 18 in. Sample wave trains are indicated in Fig. 7.

Section 2
TEST FACILITY, INSTRUMENTATION, AND PROCEDURE

The following description of the exploding-wire facility at Engineering-Physics Company (EPCO) is largely extracted from Ref. 1.

The facility was designed and constructed for the investigation of underwater explosions on a laboratory scale under the sponsorship of ONR. Its principal application has been to investigate the phenomena of bulk cavitation and the effects of underwater explosions on ships and structures. Although the system was designed to investigate explosion phenomena, it is equally well suited for the investigation of sound absorbers and radiators. The facility consists of a cylindrical tank equipped with portholes through which the underwater explosions can be observed by means of a Schlieren optical system employing both single-frame and high-speed photographic techniques. Simultaneously, pressure gages monitor the progress of shock waves, and these outputs are recorded with oscilloscopes and Polaroid cameras. In order to produce thermal, non-chemical explosions, an exploding bridge wire system has been installed. A system for timing and coordinating the sequence of events is also included. The hydrodynamic test facility is shown in Fig. 1.

HYDRODYNAMIC TEST VESSEL

The hydrodynamic test vessel consists of a near-cylindrical tank 6 ft in diameter and 6 ft high. The tank has nine portholes, two of which are 12 in. in diameter and equipped with optical flat glass windows. Five of the portholes are 6 in. in diameter and are equipped with plexiglass windows, through which instrumentation cables are fed. The remaining portholes are used in conjunction with a device for positioning the exploding-wire fixture from the exterior of the tank. A 24-in. manhole with cover is provided at the top of the tank for access. The interior of the tank is coated with an anechoic lining so that the explosions in the tank simulate a free-field test condition. The entire tank can be sealed off and fully evacuated or, alternatively,

pressurized to 54 psi. The plumbing system is provided with a filter through which water can be continuously circulated to maintain its optical qualities.

ENERGY DISCHARGE SYSTEM

An exploding-wire fixture is mounted in the tank connected via coaxial cable to a 20-kV, 15-μF, 5-nanohenry capacitor. The ringing frequency of the electrical system is about 2 megacycles, and because of the rapid energy dump, the shape of the pressure-versus-time disturbance in the water generated by the explosion is determined primarily by the characteristics of the water. A high-voltage switch initiates the explosion. Either mechanical or electronic triggering can be used. The switch discharges over a range from 2000 V or 30 joules up to 20 kV or 3000 joules. Should the need arise, additional energy-storage capacitors are available in the laboratory to increase the energy of the system to 9500 joules. A typical exploding bridge wire used in the investigation of bulk cavitation from underwater explosions is an AWG #40 nichrome wire 2 mm in length; it closely approximates a point source explosion for most applications. The exploding-wire fixture can be moved across the diameter of the vessel from the exterior of the tank, thereby providing a means for changing the location of the explosion in the tank relative to the position of the transducers and models.

SCHLIEREN SYSTEM

A 10-in.-diameter Schlieren system is incorporated in this facility and makes use of the 12-in. optical flat portholes, which are on diametrically opposite sides of the tank, as shown in Fig. 2. The Schlieren system consists of two parabolic first-surface mirrors of 80 in. focal length. Each mirror is correct to within one-quarter wavelength of mercury light. Three types of point light sources are available: (1) a steady point light source using a high-pressure mercury arc lamp; (2) a millisecond xenon flash lamp source; and (3) a 1-μsec air gap spark light source. The mercury lamp is used where phenomena of a relatively slow nature are to be studied, or for purposes of positioning models and transducers. The xenon lamp is most useful with high-

speed cinephotography for cases in which a sequence of events takes place over a period of 1 msec or less. The air gap spark is most useful where extremely high-speed events are to be monitored with the ultra-high resolution provided by single-frame, fixed-film photography. The cameras avilable with the Schlieren system consist of a single-frame 4 x 5 camera and a high-speed drum camera capable of taking a total of 224 frames per event at a shutter speed of 1 μsec with a frame separation of 40 μsec. The camera can also be run at lower framing rates with consequently lower shutter speeds and longer frame separations.

SEQUENCING EVENTS

In order to establish a sequence of events in an experiment and to correlate oscilloscope and photographic records, a number of timing circuits are required. All units can be actuated with electrical pulses. A digital time-delay generator is available which allows one to delay an input pulse from 0.1 μsec to 1 sec in increments of 0.1 μsec. A time-delay generator is available on the spark light source and on the electronic explosion-triggering circuit. Time-delay units are also avilable in the Tektronix 545 oscilloscope and Tektronix 549 storage oscilloscope. A 1-megacycle timer/counter is used for accurately establishing framing rates on the drum camera.

PRESSURE TRANSDUCERS

Three pressure transducers of the piezoelectric type are in use in the hydrodynamic test vessel. These transducers are mounted on positioners and can be located at any point on the interior of the vessel. Two Atlantic Research Type LC-10 hydrophones are available which have a sensitivity of 2300 micromicrocoulombs per psi with an open circuit voltage sensitivity of 0.3 V per psi. The transducer has a useful pressure range of 0 to 2000 psi. The LC-10 is cylindrical in shape, having a diameter of 0.38 in. by 1.13 in. in length. Two of these gages are available in the system. An Atlantic Research Type LC-5M gage is also available. This gage has a sensitivity of 11.3 micromicrocoulombs per psi and a voltage sensitivity of 0.018 V per psi open cir-

cuit. The LC-5M has a useful pressure range of 0 to 50 psi and the gage is cylindrical in shape, having a diameter of 0.1 in. and a length of 0.5 in.

SCREENED ROOM

All of the instrumentation in the test facility is enclosed in a room covered with copper screening in order to protect it from the electromagnetic radiation which results when the capacitor bank is discharged across the exploding-wire bridge. The screened room is 10 ft long, 6 ft wide, and $8\frac{1}{2}$ ft high.

TEST PROCEDURE

Each of the explosions to be described herein was generated by the release of 1690 joules of electrical energy stored as a 15-kV charge on a 15-μF condenser. The depth, length, and resistance of the exploding wire are listed in Table 1 for each shot.

Schlieren photographs were recorded on 35-mm film strips, which show the expansion of the steam bubble, the progression of the shock waves through the air and water, the motion of the water surface, and the process of bulk cavitation. The Schlieren system was used in the circular mode, i.e., with the collimated beam focused at a "point" within a circular aperture. A Dynafax Model 326, Serial No. 183, framing camera was used. The camera gave 1-μsec exposures at intervals which were nearly constant at 40 μsec, as indicated in Table 1. Some of the prints from these films are shown in Fig. 3 for five shots at various depths.

The explosively generated water waves were recorded by a 16-mm movie camera operating at a 12.07-msec framing rate. The camera, a Bolex H-16 unit, was set for operation at 64 frames/sec. However, it was calibrated at this setting by means of a General Radio Strobotac shining directly on the shutter with the lens removed. This calibration indicated the actual operating speed to be 82.83 frames/sec, or 12.07 msec/frame. Several replications of the calibration procedure show this value to be valid to an accuracy of

±1 percent. In the field of view of each 16-mm frame is a wave gage board which is scaled with 0.005-in. horizontal lines separated vertically by 0.01 in. A reflection of a mounting screw on the wave gage board appears on the water surface and may also be used to quantitatively determine the wave motion.

Shock wave pressures were monitored by oscilloscope, and Polaroid photographic recordings were made as the trace progressed in time along the face of the CRT. Sample pressure records are shown in Fig. 5. The pressure transducers were arranged in two ways. Runs 1 through 21 utilized Atlantic Research LC 10 series pressure transducers fixed at two arbitrary radial distances from the exploding-wire fixture. A length of Number 40 nichrome wire was soldered to two brass prods on the vertically mounted high-voltage probe. In the 35-mm photos, the wire end is facing downward. Runs 27 through 41 utilized three Atlantic Research Corporation LC series pressure transducers in a vertical array located at a horizontal range of 6 in. Gage designations, vertical distances below the water surface, and sensitivities were as follows:

Gage	Depth (in.)	Sensitivity (V/psi)
LC-10-2	1	0.311
LC-10-1	6	0.325
LC-5M	21	0.018

Thus the experimental data consist of three sets of photographic records: 35-mm film strips of the bubble, 16-mm film rolls of the water surface waves, and Polaroid oscilligrams of the water shock waves. Table 1 shows the identifying symbol for each test and the data records obtained. Useful data records of all three kinds were obtained for 25 of the 41 tests listed.

Section 3

PRESENTATION OF REDUCED DATA

The data reduction consisted mainly of determining the maximum cavity diameter, the maximum pressures at each of three gage locations, and the maximum wave heights.

3.1 CAVITIES

The 35-mm film strips were reproduced by use of a microfilm reader-printer that gave prints such as those shown in Fig. 3. The growth of the bubble was measured until it reached a maximum or until the film strip ended. The diameter of the bubble was measured by comparing it to the 9.5-in. diameter of the porthole through which the pictures were taken. The only difficulty encountered was that in approximately half of the records (14 out of 29), a maximum bubble diameter was not quite reached before the film strip ended. The five highest air bursts produced no measurable water cavities (i.e., they were extremely small). Hence there were 37 tests which yielded measurable cavity (or bubble) data. Eight of these tests gave unusable records, so that 29 values for the bubble diameter were obtained. In Table 2 the tests are listed by depth of burst and the 29 values of maximum (or nearly maximum) bubble diameter are indicated. These values are also plotted versus depth of burst in Fig. 4.

3.2 SHOCK WAVES

Pressure – time histories were recorded from three pressure transducers, as illustrated in Fig. 5. The sweep speeds were either 50 or 100 μsec/cm and the pressure pulses were on the order of 100 μsec in duration. This gave traces one or two divisions long. The records could have been read more accurately if the sweep speed of the oscilloscope had been faster. Also, at these low sweep speeds, the width of the trace becomes a significant percentage of the pressure pulse duration – approximately 10 percent.

Pressure transducer records were obtained for 38 out of the 41 tests, however it was difficult to obtain true peak pressures from all 38 because some of the wave forms were highly distorted from their ideal exponential shape. This was mainly due to anomalous surface reflection, as will be described later.

The pressure transducer traces were read to give directly both the maximum measured pressure and the distance between the transducer and the center of the explosion. This distance was calculated by determining the time between the detonation and the arrival of the shock wave at the gage, and multiplying this time by the speed of sound in water (4880 ft/sec). The detonation was generally indicated by a disturbance in the base line of the trace. Once this slant range is known, the peak pressure can be calculated from well-established equations, as described in the next section, for comparison with the measured data. The measured maximum pressure was corrected for gage rise time by graphical extrapolation of the exponential pressure trace back to zero time by use of a plot of the measured pressure versus time on semi-log paper, as indicated in Fig. 6. As described in Ref. 6, this calculation is usually performed by means of a computer program which selects the data to minimize gage overshoot and noise. In the manual operation employed here, human judgment was used in drawing the straight line through the data, as shown in Fig. 6. The shock arrival time, or zero time, was taken to be the time when the trace had risen to half the measured peak pressure, but this rise time could not be accurately distinguished in the oscilligrams. The measured peak pressures and the values obtained by extrapolation to zero time are presented in Table 3 for for five shots at selected depths of burst. The extrapolated values are usually about twice as large as the measured peak pressures.

3.3 SURFACE WAVES

The measured wave trains are given in Fig. 7 for eight shots: 9, 10, 16, 18, 21, 22, 25 and 28. These shots were selected to show the wave envelopes generated at depths of burst from 0 to 3.4 in. Shots 16, 18, and 28 show the extreme variation in maximum wave heights caused at shallow depths of burst by

the differences in the collapse of the cavity and plume. Comparable wa· - envelope curves predicted by theory from the measured expanded cavities (see Section 4) are also shown in these figures.

All of the shots can be considered to be in infinitely deep water, since the water depth was approximately 3 ft, which is sufficient to avoid bottom effects. The first measurable wave for all shots at the gage range of 18 in. is the trough following the collapsed lip of water. The lip became indistinguishable as it spread away from the cavity, as indicated in Fig. 4, Ref. 3. This occurrence is in agreement with deepwater detonations produced in the URS wedge tank (Ref. 3).

Only the first lobe of the surface wave envelope, and possibly the first part of the second, are obtainable from the wave gage records (i.e., 16-mm films) because the leading waves reflected off the tank wall and returned to the gage in about 3 to 4 sec, which is about the time that the waves in the second lobe of the envelope arrived at the gage.

The height of the largest crest or trough, η_m, along with its time of arrival at the gage after detonation is shown in Table 4. The largest and smallest values of peak wave height were measured for shots fired near the water surface as shown in Fig. 8. However, for Shots 36 to 40, which were detonated well above the water surface, there was no measurable cavity formation or wave generation.

Section 4
COMPARISON OF DATA WITH EXISTING THEORY AND DATA

4.1 CALCULATED YIELD AND PEAK PRESSURE

Yield

The expanded bubble diameter is shown as a function of charge depth in Fig. 4 and Table 2. For the submerged wires, this diameter was nearly constant and equal to the value for the deepest shot, i.e.,

$$D_{max} = 4.13 \text{ in. for Shot 31 at d} = 3.94 \text{ in.}$$

The expanded bubble radius is related to the explosive yield by the following well-known equations:

$$A_{max} = 11.9 \left(\frac{W_N}{Z}\right)^{1/3} \quad \text{for nuclear bursts (Ref. 7)} \tag{1}$$

$$= 12.6 \left(\frac{W}{Z}\right)^{1/3} \quad \text{for TNT charges (Ref. 8)} \tag{2}$$

where

A_{max} = maximum bubble radius (ft) = $D_{max}/2$

W = yield (lb)

Z = hydrostatic + atmospheric heads

= d (ft) + 34 for a normal atmosphere and fresh water.

Substitution of the measured values of A_{max} and d into the foregoing equations gives an equivalent nuclear yield of 0.045 gm and an equivalent TNT yield of 0.038 gm. The latter value is also obtained by the equation given on p. 50 of Ref. 2, which is equivalent to Eq. (2). The corresponding TNT charge radius is:

$$R_o = \frac{W(lb)^{1/3}}{7.32} = \frac{0.044}{7.32} = 0.0060 \text{ ft} = 0.072 \text{ in.} \tag{3}$$

For comparison with the foregoing equivalent yields based on the maximum bubble radius, the actual electrical yield can be calculated as follows:

The energy stored in the condensers for each shot was:

$$E_s = 1/2\ CV^2 = 1/2\ (15 \times 10^{-6}\ F)(15 \times 10^{3}\ V)$$

$$= 1690 \text{ joules} = 404 \text{ cal} = 1240 \text{ ft/lb}$$

The equivalent TNT charge weight is:

$$W = 404 \text{ cal } (10^{-3} \text{ gm/cal}) = 0.404 \text{ gm}$$

Thus it appears that only about one-tenth of the stored energy was put into the water. According to Buntzen (Ref. 10), this ratio is equal to the ratio of the wire resistance to the total resistance of the circuit. Hence the total resistance is estimated to have been about 10 ohms.

Peak Pressure

With known values of yield W (lb) and slant range r (ft), the peak pressure of the underwater shock wave can be calculated from the following equations:

$$P_m \text{ (psi)} = 18{,}600 \left(\frac{W_N^{1/3}}{r} \right)^{1.13} \quad \text{for nuclear bursts (Ref. 7)} \qquad (4)$$

$$= 21{,}600 \left(\frac{W}{r}^{1/3} \right)^{1.13} \quad \text{for TNT charges (Ref. 8)} \qquad (5)$$

These equations give the peak pressure for the "free water" shock wave, which is unaffected by surface reflection or any other disturbance. Values calculated from Eq. (4) are listed in Table 3. These values are at least twice as large as the extrapolated values. In some cases the ratio is much larger. This is due mainly to "anomalous" surface reflection, as will be shown next.

For submerged TNT charges the lower boundary for the region of anomalous surface reflection is shown in Fig. 9, which is copied from Fig. 4.2 of Ref. 9, where the theoretical derivation of the curves is given. In the region of

"anomalous" reflection (above the curves), the peak pressure of the water shock wave is reduced by the tension wave reflected from the water surface. The reduced depths of burst for the five shots listed in Table 3 are as follows, where the equivalent TNT charge weight is taken to be W = 0.038 gm = 0.84×10^{-4} lb, so that $(W)^{1/3} = 0.044(lb)^{1/3}$:

Shot	Charge depth, d (in.)	Reduced depth $\frac{d(ft)}{[W(lb)]^{1/3}}$
13	0.04	0.076
28	0.30	0.57
10	1.00	1.9
9	2.35	4.4
31	3.94	7.5

The three pressure gages were located at the following nominal reduced values of horizontal range and depth:

Gage	Horizontal Range, X (in.)	Depth, Y (in.)	$\frac{X(ft)}{[W(lb)]^{1/3}}$	$\frac{Y(ft)}{[W(lb)]^{1/3}}$
LC-2	6	1	11.4	1.9
LC-1	6	6	11.4	11.4
LC-5	6	21	11.4	39.7

By use of the foregoing values in Fig. 9 one finds that for the data listed in Table 3, both gages were in the anomalous region for the shallowest shot, Shot 13; and for Shot 28, the highest gage was near the anomalous region. All the other measured values of peak pressure listed in Table 3 should not have been reduced by the influence of surface reflection. Nevertheless, these values (extrapolated) are about half as large as calculated, except for the deepest gage (LC-5 at a depth of 21 in.), which consistently indicated extremely low pressures.

4.2 CALCULATED SURFACE WAVE TRAINS

In order to predict the surface wave trains theoretically, the following system of equations in dimensionless form was programmed to compute a wave gage record (η versus t) for given measured values of water depth, initial cavity radius, and gage range. The derivation of the equations is given in Ref. 3. The final equation for the wave height η at range R and time t can be expressed as:

$$H = FG \cos \theta \tag{6}$$

where

$$H = \sigma^2 \frac{R\eta}{R_c d_w} \tag{7}$$

$$F = \text{a function of } \sigma = \sqrt{\frac{\sigma\phi(\sigma)}{-\phi'(\sigma)}} \tag{8}$$

$$2\phi = 2R/\sqrt{g d_w}\ t \tag{9}$$

$$= \sqrt{\frac{\tanh \sigma}{\sigma}} + \frac{\sqrt{\sigma/\tanh \sigma}}{\cosh^2 \sigma}$$

$$\sigma = \text{an independent variable defined by Eq. (13)} \tag{10}$$

$$G = \text{a function of the cavity shape and } \sigma \tag{11}$$

$$\theta = 2\pi\left(\frac{t}{\tau} - \frac{R}{\lambda}\right)$$

$$\lambda = \text{wavelength} = \frac{2\pi d_w}{\sigma} \tag{13}$$

$$\tau = \text{wave period} = \frac{2\pi}{\left(\frac{g}{d_w}\sigma \tanh \sigma\right)^{1/2}} \tag{14}$$

$$t = \text{time from release of cavity (sec)} \tag{15}$$

$$R = \text{horizontal range from charge (ft)} \tag{16}$$

$$R_c = \text{cavity radius at water line when cavity depth is maximum (ft)} \tag{17}$$

$$= 1/2\ D_{max} \text{ for deep shots by assumption}$$

$$d_w = \text{water depth (ft)} \tag{18}$$

$$g = \text{acceleration of gravity } (32.2 \text{ ft/sec}^2)$$

The "deepwater" wave trains are assumed to originate from an initially motionless cavity shape represented mathematically by a parabola with a raised lip (giving zero net displacement) and a depth both equal to the horizontal radius, R_c, as shown in the following sketch. For the deeply submerged shots ($d > \frac{1}{2}D_{max}$), it is assumed that the bubble breaks through the surface and gives a motionless cavity with $R_c = \frac{1}{2}D_{max}$.

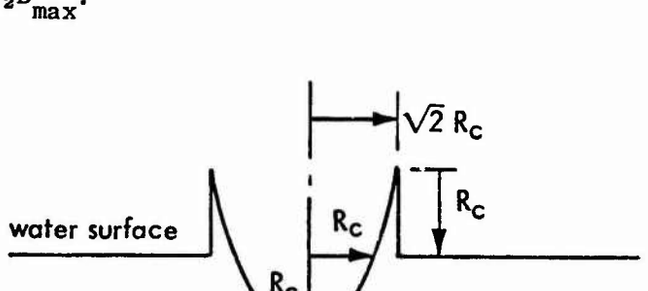

Analytical Cavity Shape

For this cavity shape:

$$G = -\sigma_b J_3(\sigma_b) \tag{19}$$

where

$\sigma_b = \sqrt{2}\, R_c \sigma / d_w$

$\bar{\eta}_c$ = the zero-order Hankel transform of the above cavity shape

J_n = Bessel function of the n^{th} order

Also for this cavity shape and for "deep water", where $d_w > 5R_c$, the length of the peak wave is constant ($\lambda_m = 2.1R_c$), and the height of the first lobe of the wave envelope at any range is given by the first theoretical value below (from Table 6, Ref. 3), which also corresponds to the theoretical peak wave height when there is a wave peak located at the peak of the first lobe of the envelope.

$R\eta_m / R_c^2$	d_w / R_c
0.89	>>1
0.86	2
0.78	1
0.47	1/2

The foregoing theoretical values show that the peak wave height does not decrease much with water depth until the water becomes so shallow that the cavity touches bottom ($d_w \leq R_c$).

Comparison With Measured Data

Wave trains computed from the FORTRAN program are compared with measured wave trains for eight shots in Fig. 7. The time scales for all shots are measured from detonation of the charge, whereas the time for the theoretically predicted wave trains starts with the release of the expanded cavity. Each pair of calculated and measured wave trains was matched by adding a constant time increment T to the computed value of t and by multiplying the calculated peak wave height by the factor K. The constants T and K are chosen so that the maximum calculated wave is superimposed on one of the more prominent measured waves (usually the largest wave), as shown in Fig. 7. The empirical values of T and K are listed in Table 5. The value of K generally ranges between 0.10 and 0.25, as shown in Fig. 10, where the values from Table 5 are plotted versus charge depth. The trend is somewhat consistent for submerged shots, whereas the surface shots transmitted more energy into the waves, hence greater K. Two shots, 16 and 18, are exceptions because of differences in cavity and plume collapse, which will be discussed in Section 5. Although one might expect T to equal the time for cavity formation, the actual values are much larger than this time, which was only about 0.005 sec.

Comparison of the calculated and measured wave trains is satisfactory after the application of the factors K and T. Although the measured wave crests and troughs fall reasonably well on the calculated wave envelopes, the measured wavelengths are consistently somewhat larger than calculated.

4.3 PREVIOUS DATA

NRDL Exploding Wire Data

Experiments were conducted at the Naval Radiological Defense Laboratory (NRDL) from about 1962 to 1964 with submerged exploding wires, mainly to investigate the distribution of explosion products. Some of the reports on these tests are listed as Refs. 2 and 10 through 13. Some of the results obtained at NRDL are of interest here since they are comparable with the EPCO data.

Buntzen reported the following results in Ref. 11. With an initial voltage of 25 kV across a 5.76-μF condenser, the stored energy was:

$$E_s = \tfrac{1}{2} CV^2 = 1800 \text{ joules} = 430 \text{ cal}$$

Buntzen reported that this was equivalent to 1.64 gm of TNT; however, at 1000 cal/gm, the equivalent charge weight would be 1.72 gm of TNT. This stored energy was only slightly greater than that for the EPCO tests (Section 4.1). A 1-in.-long copper wire was exploded at a depth of 2 ft in a vacuum tank partially filled with water under an air pressure equivalent to 4.48 in. Hg, or 5.08 ft H_2O. The wire resistance was 0.025 ohms and the resistance of the total circuit was 0.065 ohms, so that the energy put into the wire (or the equivalent explosive yield) was $\frac{0.025}{0.065}$ (1800) = 693 joules = 165 cal = 0.165 gm TNT, or about 4 times greater than that for the EPCO tests.

The maximum bubble radius was 0.44 ft, and the corresponding charge weight from Eq. (2) is 0.137 gm TNT, which agrees well with the previous (electrical) value. The peak pressure of the water shock wave was measured at a distance of 22.8 in. and found to be 225 psi. The value calculated from Eq. (5) with W = 0.137 gm = 3.02×10^{-4} lb TNT is 490 psi. Hence the measured peak was somewhat less than half the calculated value, just as for the EPCO data (Section 4.1). Buntzen reported that smaller wire resistance gave lower equivalent yields, and this will be discussed further in Section 5.

Buntzen (Ref. 11) reported that in his tests the distribution of energy was as follows:

Bubble (31.0%)	214 joules
Shock wave (9.2%) and shock dissipation (53.6%)	435
Thermal radiation (6.2%)	41
Total (100%)	693 joules

However, Hege later reported (Ref. 12) that the thermal radiation measured for two exploding wires amounted to 270 and 209 joules, respectively, or 39 percent and 30 percent of the total energy. This would reduce the estimated energy dissipated by the shock wave to about 20 percent of the total.

In a later report (Ref. 13), Buntzen described the results for 15 repeat shots with a submerged 10-mil gold wire, $\frac{1}{4}$ in. long. The maximum bubble radius ranged between 11.1 and 13.9 cm and the first bubble period ranged between 50.3 and 62.8 msec.

In the most recent of the series of NRDL reports on exploding wires (Ref. 2), Pritchett gives an extended discussion of vacuum scaling and reports that for submerged wire explosions, the equivalent TNT charge weight (gm) usually corresponds to a value between 0.6 and 1.0 times the electrical energy released to the wire (Kcal). This ratio depends on the circuit parameters and assumes that the energy released by TNT charges is 1 Kcal/gm.

The values reported by Buntzen (Ref. 11) give the following ratios:

$$\frac{\text{energy released to wire}}{\text{stored energy}} = \frac{165 \text{ cal}}{430 \text{ cal}} = 0.38$$

and based on the maximum bubble radius

$$\frac{\text{equivalent TNT energy}}{\text{energy released to wire}} = \frac{137 \text{ cal}}{165 \text{ cal}} = 0.83$$

The latter value agrees very well with the TNT/nuclear equivalence from Eqs. (1) and (2), i.e., $(11.9/12.6)^3 = 0.85$.

The energy ratio of the equivalent TNT charge to stored electrical is 137/430 = 0.32, which is about 3.4 times higher than the ratio for the EPCO tests (0.094). Apparently the effective load resistance was small because of the short wire gap for the EPCO tests. Pritchett reported values ranging between 0.7 and 1.1 for the ratio of equivalent TNT to released energy for tests with wires 1.2 in. long. For one shot the calculated electrical yield was 0.138 gm TNT at a depth of 29 in. in water under 0.015 atm of air pressure. The equivalent yield based on the maximum bubble radius was 0.134 gm TNT ±0.013. For 34 repeat shots the bubble radius ranged between 6.58 and 7.33 in., and the corresponding yield ranged between 0.109 and 0.151 gm TNT. The repeat shots in Table 2 indicate about the same repeatability.

URS Vacuum Tank Data

An extensive series of tests was conducted by Kaplan, et al. with small HE charges submerged in an oil tank with normal atmospheric pressure and with the atmospheric pressure reduced as low as 0.003 atm (Ref. 5). Three different HE charges were used with yields (based on the maximum bubble radius) of 0.054, 0.17, and 1.57 gm of TNT. Shots were fired over wide ranges of charge depth and water depth. High-speed movies were taken of the cavities and bubbles, and the water surface waves were measured with electronic wave gages.

For the smallest charge the dimensions of the expanded cavities are shown in Fig. 11, where the values were measured when the depth of the cavity, D_c, was maximum. The corresponding curve for cavity radius, R_c, is also shown for the EPCO exploding-wire tests (i.e., $D_{max}/2$ vs d from Fig. 3). It is evident that the R_c vs d curve for this smallest charge and for the exploding wire are both nearly flat for $d > \frac{1}{2}$ in. However, as the two explosive sources approach the water surface from below, the two curves diverge. This indicates that the TNT equivalence of the wire (or line source) explosions decreases for near-surface bursts, as has been suggested before by many authorities for nuclear (or point source) explosions. It can also be seen from Fig. 11 that the cavities become elongated ($D_c > R_c$) for the HE shots at

shallow charge depth and for normal atmospheric pressure. This effect was also very prevalent for the 1-lb TNT charges fired by Hendricks of NRDL (Ref. 15) as shown in Fig. 64 of Ref. 3. The effect did not occur under vacuum, however, as shown by the upper two curves in Fig. 11. There is also no evidence of the elongation effect for the exploding wire (i.e., $R_c \simeq D_c$ in Fig. 3).

The data for water surface waves measured under vacuum by Kaplan, et al. are shown in Fig. 12. It can be seen from Fig. 7 that for the EPCO tests, the second wave crest was always the highest and nearly equal to the height of the first lobe of the wave envelope under normal pressure, just as reported by Kaplan (and indicated in Fig. 12) for the HE charges under vacuum. The horizontal range of the wave gages was the same for both test series, i.e., R = 18 in. For the EPCO data this range was sufficient, according to Ref. 3 (i.e., $R > 5\ R_c$ where R_c = 2 in.), to insure that the wave trains were stable. However, for the HE data this was not the case, since $R_c > 4$ in. even for the smallest HE charge under vacuum (Fig. 11). Nevertheless, for this charge the following values were measured at d = 0 and P_a = 0.003 atm (Fig. 11):

$$R_c \simeq D_c \simeq 5.5 \text{ in.}$$

and

$$\eta_m R \simeq \tfrac{1}{2} \times 18 \text{ in.}^2$$

These values give the ratio

$$\frac{\eta_m R}{R_c^2} = \frac{9}{(5.5)^2} = 0.30$$

The latter ratio is proportional to the square root of the ratio of the energy in the wave train and in the initial cavity. Theoretically $\eta_m R = 0.89\ R_c^2$ for no energy losses (Ref. 3). The measured ratio compares well with the ratios for the three repeat shots at the surface under normal pressure with the exploding wire, i.e., 0.22, 0.32, and 0.21 in Table 4. Hence the collapse of all these nearly hemispherical cavities and the generation of surface waves apparently "scaled" even though the atmospheric pressures were vastly different.

Comparison With Other HE Data

The latter three values and the others listed in Table 4 are plotted in Fig. 13 versus the ratio of charge depth to the equivalent TNT charge radius, d/R_o. Similar plots are shown in Fig. 13 for shots in the URS wedge tank, where 1-lb TNT charges were simulated (Ref. 3), and for the 9200-lb TNT charges fired at Mono Lake in 1965 (Ref. 14). It appears that the EPCO data scale with the Mono Lake data at least as well as the wedge tank data. All three plots show the upper critical depth (UCD) effect, i.e., a peak in wave height when the TNT charge (or its equivalent) is slightly less than completely submerged. However, the effect is more distinct for the exploding wire than for the HE charges. This is the first direct experimental evidence that the UCD depth effect occurs for "nuclear" as well as for HE bursts.

Further comparison of the exploding-wire data is given in Fig. 14, where the EPCO data are reduced and compared with the data and curves in Fig. 2 of Ref. 14. Again the UCD effect is most evident for the wire data. The similarity between the EPCO and Mono Lake wave data versus charge depth for the shallow shots is very striking, and the scaling laws appear to hold extremely well even over the very large range of yield (10^{-6} to 10^{4} lb of TNT). The EPCO data appear to fit within the dashed TNT band (which is based on a great deal of data generated mainly by the U.S. Army Waterways Experiment Station [WES]), even better than the Mono Lake data. This may have been caused by the attraction of the submerged explosion bubbles to the bottom of Mono Lake, since the deepest charge was fired at a depth of 51 ft in water 130 ft deep and gave a column diameter of 160 ft (Ref. 15). Thus the water was probably not deep enough to avoid bottom effects for the deeper Mono Lake shots.

Section 5
DISCUSSION OF EPCO DATA

REPEATABILITY

The effect of the electrical resistance of the exploding wire is shown by the following list of values extracted from Tables 1 and 2 for shots repeated at the same depth.

Shot No.	Wire Depth, d (in.)	Resistance of wire (ohms)	Cavity Diameter, D_{max} (in.)
34	-0.39	0.9	1.63
35	-0.39	1.19	1.45
12	0	0.8	3.37
32	0	0.97	3.19
21	0	1.17	3.37
17	0.09	0.78	3.80
19	0.09	0.86	4.07
18	0.09	1.18	4.21
30	0.10	0.96	4.11
20	0.10	0.96	4.20
4	1.0	0.98	4.12
10	1.0	0.83	4.15
8	2.0	0.72	3.82
25	2.0	0.8	4.28
2	2.0	0.815	3.99
41	2.0	0.9	4.42
		(from Table 1)	(from Table 2)

It can be seen that the longer wires (with greater electrical resistance) tended to give somewhat larger cavities (or yields) in agreement with Buntzen's

results (Ref. 11). However, the cavity diameter varied less than 15 percent for the repeat shots even with the variation in wire resistance.

The measured values of cavity diameter show comparatively little scatter at shallow depths (Fig. 4). However, there is a great deal of apparent scatter* in the plot of peak wave height versus charge depth, particularly at shallow charge depths (Fig. 8). For example it can be seen from these two figures that Shot 18 was fired slightly deeper and gave a cavity 1.19 times larger than Shot 16. However, both repeat shots (15 and 16) gave a peak wave four times higher than Shot 18.

UPPER CRITICAL DEPTH

The erratic behavior just described, and its similarity to that observed for HE charges, strongly suggests the presence of a UCD effect. Since the present data are the only existing direct experimental evidence that the UCD effect occurs for "nuclear" as well as for HE bursts, further discussion seems warranted. The present data are more complete than for any other test series since they show in detail (versus the charge depth) how the following related phenomena vary with time: detonation, cavity and plume expansions, air shock, water shock, shock reflection, and bulk cavitation. Thus it was hoped that careful examination of the data might show the physical cause for the UCD effect; however, there is only a little new information to report, as will be described next.

For three of the shallow shots, the equivalent TNT charge, the charge depth, and the expanded cavity and plume are all shown to scale for comparison in Fig. 15. An even shallower shot is shown in Fig. 3a. All four of these cavities were still expanding slowly at the time of the last frame of the movie; however, they were nearly fully expanded. Comparison of these four (nearly) expanded cavities and columns indicates that all of the

*This scatter is also evident in comparable plots for HE charges weighing between $\frac{1}{2}$ and 10^4 lb which have been fired by WES and others (Fig. 14).

cavities were nearly hemispherical, and that the cavity diameter increased slightly with charge depth. However, for Shot 16 the peak wave height was at least twice as large as for all the other shots. For this shot (and the repeat shot, 15) the equivalent TNT charge was slightly protruding through the water surface, since the charge depth was 0.06 in. and the radius was 0.072 in. This is near the typical location of an HE charge for maximum wave generation, i.e., the UCD effect. For example, in Figs. 13 and 14 the UCD was obtained for the Mono Lake charges, (with a radius of 2.84 ft) when the charge depth was 1.04 ft.

It is apparent from Figs. 15 and 7a that the expanded water column was nearly vertical for Shot 16, but tapered inward for the other three shots. Examination of Figs. 7a, b, c and d does not indicate any anomolous feature of the wave train for Shot 16 except that the wave peaks are higher.

Thus the only distinguishing feature of Shot 16, in addition to the higher waves, was the vertical column walls. Unfortunately the framing camera ran out of film before the cavity and column collapsed to generate waves. However, additional pictures showing the subsequent collapse of the plumes and cavities could be obtained readily by repeating a few shots with a slower camera viewing the explosion.

The photographic data in Ref. 4 show that all of the Mono Lake shots fired near the surface (in the 1965 series) gave nearly vertical water columns, and the shot giving the largest column diameter was somewhat deeper than the UCD. This same effect is shown in Fig. 16, where the cavity diameter, the peak wave height, and their ratio are plotted versus charge depth for the EPCO shots near the water surface.

The columns and plumes photographed by Hendricks (Ref. 15) for 1-lb HE charges also became tapered inward as they expanded, as shown in Fig. 64 of Ref. 3. This was caused by the inward collapse of the walls due to overexpansion of the cavity to a pressure much lower than the ambient pressure. The consequent "blow in" caused a downward jet to impinge on the bottom of the cavity and subsequently elongated it. There is some evidence of the

onset of this impingement in a few of the last frames of the EPCO framing camera films of the expanded cavities (not shown herein) since the surfaces of these cavities occasionally become slightly roughened.

LOWER CRITICAL DEPTH

The lower critical charge depth for surface wave generation occurs when the bubble breaks through the water surface just before it becomes fully expanded. The lower critical depth is slightly less than the bubble radius, or about 2 in. for the EPCO tests, as is quite evident in Fig. 8.

SCALING

The cavity radius R_c appears to be nearly equal to the submerged bubble radius, i.e., $A_{max} = D_{max}/2$ in Eq. (2). This is shown directly by Fig. 4 for the shallower shots, where the cavity was formed while the camera was running. For the deeper shots, the submerged bubble vented considerably later than the time of the last picture. For these shots it is assumed that the venting bubble forms a nearly motionless hemispherical cavity with radius $R_c = A_{max}$. This assumption is supported by the photographic data in Refs. 15 and 16 and by the reasonable agreement between the measured wave trains and those calculated based on this assumption (Fig. 7h). The assumption also appears to be borne out by the data for CROSSROADS-Baker, for which the measured column diameter and the value of A_{max} calculated from Eq. (1) for a yield of 20 kt are both slightly less than 1,000 ft (Ref. 16). However, the charge depth (90 ft) and the water depth (180 ft) were so much smaller than A_{max} that the hypothetical "free-water" bubble never actually formed, except for a small portion which formed in the water that was present.

The peak wave heights generated by the exploding wires appear to scale well with Mono Lake and other HE data when the standard scaling rules are applied, as shown in Fig. 14.

Capillarity (or surface tension) begins to increase the celerity and frequency) of gravity waves appreciably when the wavelength becomes less than

about 2 in. (or the period less than about 0.17 sec). All of the measured waves were longer than this except for those generated by the small cavities caused by the airbursts. Although capillarity effects were small in the EPCO tests, they could be reduced further by reduction of the atmospheric pressure in the test chamber and/or increasing the wire yield, so that larger cavities and waves are generated (Fig. 11).

The measured values of peak pressure for the underwater shock wave were about half as large as predicted by the standard equations [Eqs. (4) and (5)], which are empirically derived and theoretically supported. The same result was reported by Buntzen for a more powerful exploding wire (Ref. 11). This difference may be due to inaccuracy of the predictive equations for the small yields of the wires, higher dissipation rates for the thinner shock waves generated by the wires, and/or measurement errors associated with the thin shock waves.

Comparison With Theory

The water surface waves predicted theoretically for an initially motionless, nearly hemispherical cavity (with radius R_c equal to the measured value of A_{max}) appear to be in reasonable agreement with the measured wave trains when the empirical coefficients K and T are applied. For no energy losses during the collapse of the cavity and the generation of the waves, the Kranzer-Keller theory predicts a peak wave height given by $\eta_m = 0.89\ R_c^2$. The measured data indicate values about one-third as large for near-surface bursts (Fig. 13). Thus it appears that only about one-ninth of the energy in the expanded cavity propagates away as water surface waves, and that the balance is dissipated as turbulent losses in the spilling breakers, which are generated out to about 5 cavity radii, as described in Ref. 3. Such losses are inevitable even in deep water because the theoretical peak wave is so steep near the cavity (i.e., higher than 15 percent of the wavelength) that it is hydrodynamically unstable and must spill over as observed (Ref. 3). The result of this energy loss can be accounted for by use of the empirical coefficient K, as described in Section 4.2 and shown in Fig. 10 and Table 5. For the

airbursts (Shots 33, 34, and 35 in Table 4) the measured data give the following values: $R\eta_m/R_c^2 = 0.508$, 0.802, and 0.850. The latter two values are only slightly less than the theoretical value for no energy losses (0.89), and the cavity data are reliable since these three cavities did become fully expanded during the photographic coverage (Table 2). Thus it appears that even though these shots generated smaller cavities than the submerged shots, nearly all of the energy in the smaller cavities was conserved and propagated as water surface waves. The effects of capillarity, as described previously, may have caused this apparent increase in hydrodynamic stability, since such an increase does occur under different circumstances (Ref. 16).

Nuclear Equivalence

The exploding wire cannot be expected to duplicate in detail the hydrodynamic effects of a submerged nuclear explosion. This is immediately apparent from the fact that the wire used in the tests described herein was not a "point" source but a "line" source, with a length nearly equal to the diameter of the equivalent TNT sphere. However, there is some indication that the exploding-wire (line) source more closely approximates the nuclear (point) source than the HE (spherical) source. This indication is shown in Fig. 11, where the cavity radius is shown to decrease as the wire depth of burst approaches the water surface from below, whereas just the opposite trend is evident for the HE charge (both fired under normal atmospheric pressure). This decrease in TNT equivalence at shallow charge depths has often been pointed out as being likely to occur for nuclear explosions because of radiation losses to the air. However, it is not certain whether the effect was caused here by this mechanism or by a difference in the expansion of the HE detonation gases and the steam generated by the wire.

Another way that the wire explosion might be compared to nuclear and HE explosions is by examination of the "cross-over" radius, where the water shock wave advances in front of the air shock wave. The shock fronts are estimated to cross over at about 24 charge radii for a surface burst, based on the comparison of the radius of the shock front for a spherical TNT charge in air

(Ref. 18) with the radius of the water shock wave, which advances nearly at the speed of sound in water (4880 fps) except within about 3 charge radii. The cross-over radius is somewhat larger for nuclear explosions due to the fact that at short ranges, the air shock wave is stronger than that produced by HE explosions. The cross-over radius is 28.4 times as large as the equivalent TNT charge radius for a 1-Mt nuclear surface burst, based on the calculated results in Ref. 19 and the previous (sound speed) approximation for the water shock front. The measured data for the time of arrival of the air shock front (near the surface) for seven nuclear surface bursts indicate that the shock waves cross over between 17 and 40 equivalent TNT charge radii. Hence the measured data agree with the predicted value within the scatter of the data.

The measured shock front radii for the exploding wire shots at zero depth are shown in Fig. 17. The water shock waves were hemispherical and fell very close to the straight line indicated. The detonation time was found by extrapolation of this line to zero radius. Then the measured air shock radii were plotted versus time as indicated. The vertical radius of the air shock front was consistently somewhat larger than the horizontal radius, as indicated in Figs. 7 and 17. The cross-over radius (where $R_H = R_{ws}$ in Fig. 17) is estimated to be about 1 in., (although there is considerable uncertainty in this value). This would correspond to about 14 equivalent TNT charge radii, which is closer in than would be the case for large TNT or nuclear explosions. Hence the data are not accurate enough to distinguish between a "nuclear" and an "HE" source.

Section 6
CONCLUSIONS AND RECOMMENDATIONS

The following conclusions are based on the data obtained at Engineering-Physics Company with wires exploded in water under normal atmospheric pressure and on the comparison of these data with previous theory and data.

CONCLUSIONS

1. The high-speed Schlieren photography shows nearly all the hydrodynamic effects which occur close to the exploding wires at early times.

2. For repeat shots at the same depth, the diameter of the expanded bubble (or cavity) varied as much as 15 percent, which is consistent with previous test results obtained at NRDL. The bubble diameter was about 4.1 in. and the equivalent TNT charge weight was about 0.038 gm = 0.84×10^{-4} lb.

3. The near-surface shots generated cavities which were nearly motionless and hemispherical when they become fully expanded.

4. The bubble (or cavity) diameter was nearly independent of the charge depth, thus agreeing with previous data for small HE charges; but the diameter decreased sharply as the wire approached the water surface from below. This indicates a decrease in the equivalent TNT yield for shallow charge depths, which has been predicted to occur for nuclear explosions because of radiation losses to the atmosphere.

5. With the wire located at the water surface, the water shock wave apparently advanced in front of the air shock wave at roughly 10 equivalent TNT charge radii. This cross-over occurred closer in than is the case for either large HE or large nuclear surface bursts.

6. In agreement with previous NRDL exploding wire data, the peak pressure of the free-water shock wave (outside the region of anomalous surface reflection) was about half as large as predicted by the empirical equations

for either HE or nuclear underwater explosions. This may have been caused by the extremely small yield, higher dissipative losses, or measurement errors.

7. The curve for peak wave height versus wire depth for the water surface wave trains scales very well with previous data for HE charges as large as 10^4 lb, even though the equivalent TNT charge weight for the wire was only 10^{-4} lb.

8. A very sharp peak in wave generation occurred when the wire was located at the upper critical depth, where the equivalent TNT sphere protruded slightly through the water surface. This is the first direct experimental evidence of this effect for other than HE explosions. The only clue to the physical cause of this effect was that the walls of the expanded water column tapered inward less at the critical wire depth than at other depths. The lower critical depth is also apparent in the measured data.

9. The measured wave trains compare reasonably well with those predicted theoretically for an initially motionless, nearly hemispherical cavity if empirical coefficients are used to correct the theoretical predictions for a time lag and for energy losses during the collapse of the cavities into turbulent breakers within about 5 cavity radii (as observed previously in the URS wedge tank. See Ref. 3).

10. For the submerged wire shots, apparently less than one-ninth the potential (or gravitational) energy in the expanded cavities was not dissipated close to the cavity, and was propagated away as stable water-surface wave trains.

11. For shots at low heights of burst (above the water surface), relatively small hemispherical cavities were generated, about 1.5 in. in diameter. These small cavities were extremely efficient in transmitting their energy into wave trains. The increased stabilization by surface tension (for the shorter waves generated by the smaller cavities), may have prevented the formation of spilling breakers near the cavity. This would have caused this efficient energy transfer.

RECOMMENDATIONS

Additional experiments, listed below, are recommended to check and expand the results already obtained at EPCO and reported herein.

The new experiments, although useful in their own right, will provide further understanding of the capabilities of the exploding wire for simulation of nuclear explosions. The Schlieren optics used in the facility enable one to follow the progress of direct and reflected shock waves in the water and in the overlying air, and to observe bottom effects and surface effects. Phenomena and effects peculiar to nuclear-like, steam-bubble explosions can be investigated. Data correlating the generation of surface waves, plumes, and air blast can be obtained at relatively low cost. A variety of reflecting bottoms (both in respect to contour as well as reflectivity) can be studied. The atmospheric pressure in the test chamber can be reduced, and the present 3-kilojoule energy capacitor can be paralleled to increase the scale of the yield considerably.

Additional Experiments Recommended

1. Repeat some of the shots, with slower cameras (in addition to the Schlieren framing camera) viewing the explosions at a wider angle.

2. Repeat some of the shots with the tank evacuated nearly to the flashing point of water.

3. Repeat some of the shots, particularly at low heights of burst, with the probe and/or the wire mounted both horizontally and vertically for comparison with the previous data.

4. Repeat some of the shots with a flat steel plate as a false bottom under the wire to simulate 5 nuclear explosions in shallow water, where the cavity hit bottom as it expanded.

5. Run series of tests with the wire located both at the water surface and at the upper critical depth over the false bottom (described in Item 4) with the water depth reduced to very small values.

The purpose of Item 1 is to obtain a wider view of the explosions at later times. This will allow measurement of the plume height and will show the cavity collapse, jet impingement on the bottom of the cavity, and the spilling breakers which are believed to occur out to about 5 cavity radii. The physical cause of the upper critical depth effect and its correlation with plume height and airblast could be studied.

The purpose of Item 2 is to obtain larger bubbles and cavities, and hence larger and higher peak water waves. This will alleviate the effects of surface tension and allow more accurate wave measurement. The data reported herein indicate that the shape of the water column and its collapse may be the primary cause for the upper critical depth effect. Reduction of atmospheric pressure would give further information on this, and will allow improved scaling of large explosions.

The main purpose of Item 3 is to explore the cause of the very rapid decrease in cavity size with charge depth for explosions near the water surface, as depicted in Figs. 4 and 11. This decrease is much more rapid than that which occurs with HE charges, and it is not clear now whether it is a "real" effect, ascribable to the absence of detonation products for a "point" explosions, or if it is caused by the electric arc being extinguished by the air shock wave reflected off the water surface.

Item 4 is intended to demonstrate how well the exploding wire can simulate the known effects of five underwater nuclear explosions.

Item 5 should give data to indicate whether the upper critical depth effect occurs in shallow water. Additional data correlating the generation of water waves, water columns, and air blast in shallow water would be obtained to augment the previous data for deep water.

The overall objective of the recommended experiments is first to demonstrate how accurately the effects of five nuclear explosions can be simulated by the exploding wire facility, and then to obtain additional

data for other combinations of charge depth and water depth to correlate the phenomenology of the generation of water waves, water columns, and air blast.

Recommended Modifications to the Experimental Facility

For additional tests, four changes in experimental arrangement are recommended:

(1) Addition of a framing camera having a speed of about 2500 frames/sec and other, slower cameras viewing surface effects outside the Schlieren light path

(2) Addition of a vacuum pump to reduce ambient pressure

(3) Installation of a false bottom

(4) Installation of thin surface wave rods

The present framing camera, operating at 25,000 frames/sec, provided useful information on the early stages of bubble growth and initial shock propagation in the water and in the air. It would be helpful to have the total duration of information continue out in total elapsed time by a factor of 10 to 20. This can be done conveniently with a Fastax camera operating at 2500 frames/sec. Since this Fastax photography is to be taken in parallel with the existing arrangement, a partially silvered mirror will be installed in the optical path so as to divert, say, 20 percent of the light to the Fastax; the remaining 80 percent of the light will be adequate to operate the present 25,000-frames/sec camera.

Ultimately, by using oil (instead of water) for the liquid medium and pumping the air pressure down to 0.003 atm, the conditions achieved by Kaplan for HE explosions could be reproduced. Initially it will be sufficient to pump down nearly to the vapor pressure of water (about $\frac{1}{2}$ psia or 1/30 atm at laboratory ambient temperature). The volume of the test chamber is approximately 150 cu ft. A vacuum pump capable of pumping down this large volume in a reasonable time (say, half an hour) would prevent undue delays

between tests. It is recommended that a pump capable of achieving the desired final pressure with oil, but which can be used meanwhile with water, be procured.

It is recommended that a hard false bottom be added to allow augmentation of the data for deep water reported herein.

The surface-wave data were obtained by measuring (with a relatively slow-speed camera) the wave height against a calibrated plate in a radial plane. These data were compromised somewhat by surface tension effects at the plate. It is recommended that the plate be replaced with thin calibrated wave rods in order to minimize surface tension effects.

Section 7

ILLUSTRATIONS AND TABLES

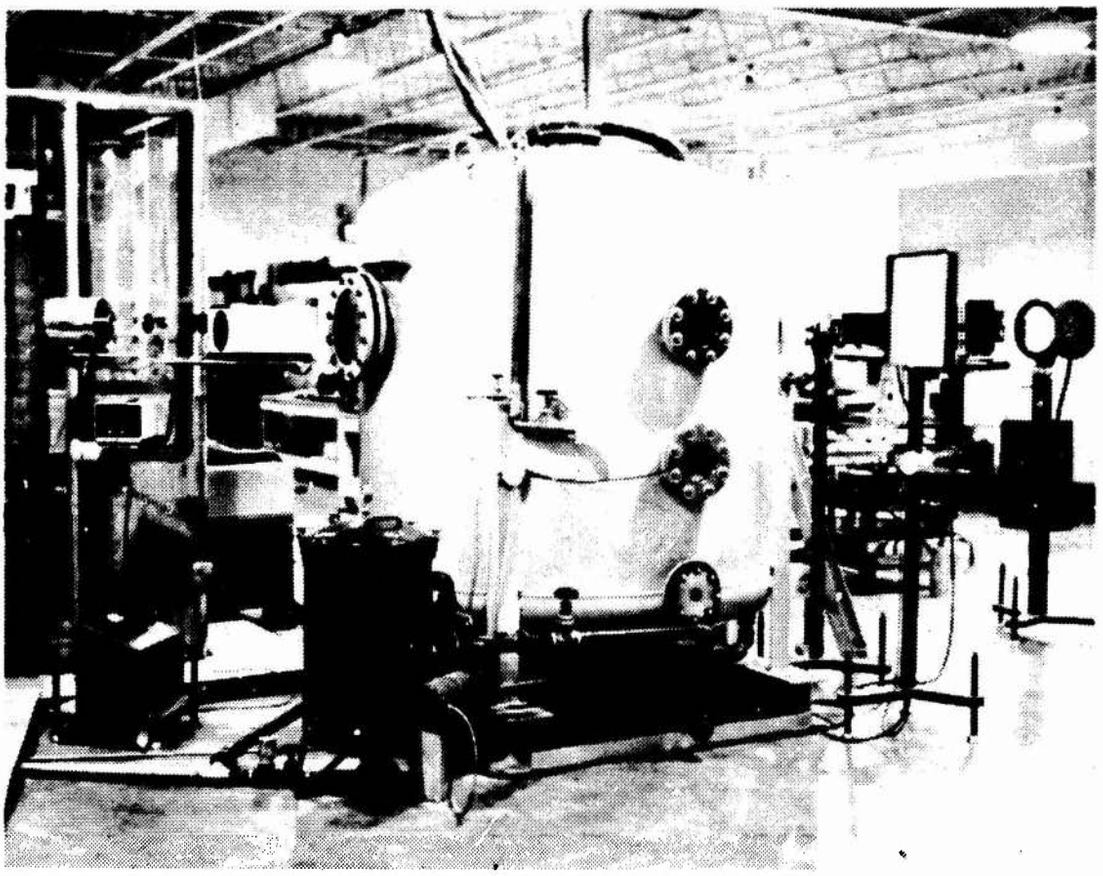

Fig. 1. Test Chamber and Schlieren Optical System

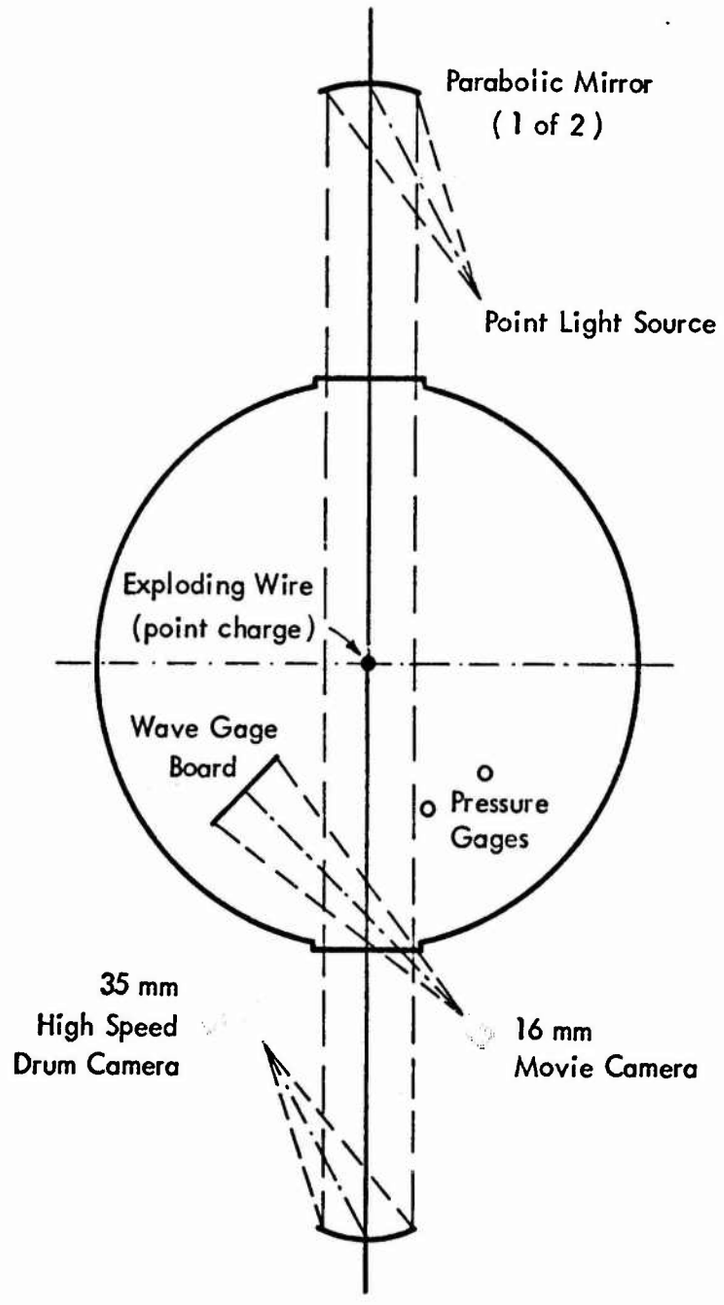

Fig. 2. Test Setup and Optical System

Figure 3

Cavities, Bubbles, Columns, Plumes, Domes, and Shock Waves from Submerged Exploding Wires at Five Depths of Burst

NOTE: Numerals adjacent to photographs denote frame number.

Fig. 3a, Shot No. 13, Code No. 0218693

Framing interval, (μsec)	=	40.5
Wire length (mm)	=	2.4
Wire resistance (Ω)	=	0.69
Water depth, d_w (in.)	=	36
Shot depth, d (in.)	=	0.04
Expanded cavity radius, R_c (in.)	=	1.71
Expanded cavity time, t_c (sec)	=	-
Wave gage range, R (in.)	=	19
Peak wave height, η_m (in.)	=	0.030
Arrival time for peak wave, t_m (sec)	=	2.60
Empirical ratio, K	=	-
Empirical time shift, T (sec)	=	-
$\frac{R\eta_m}{R_c^2}$	=	0.195

679-6

SHOT 13

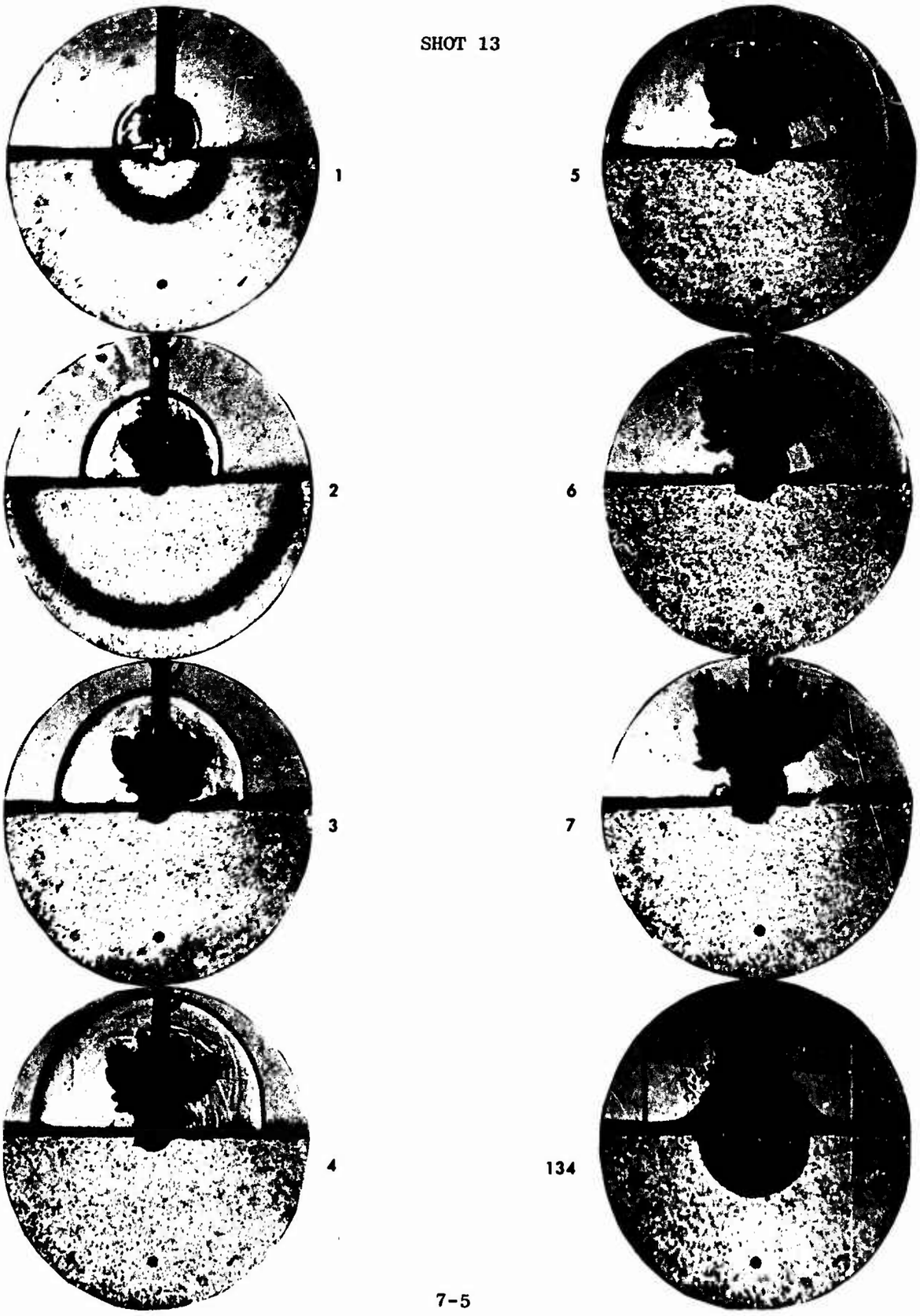

Fig. 3b, Shot No. 28, Code No. 0310691

Framing interval, (μsec)	=	40.5
Wire length (mm)	=	3.6
Wire resistance (Ω)	=	1.12
Water depth, d_w (in.)	=	36
Shop depth, d (in.)	=	0.30
Expanded cavity radius, R_c (in.)	=	2.39
Expanded cavity time, t_c (sec)	=	0.0073
Wave gage range, R (in.)	=	19
Peak wave height, η_m (in.)	=	0.025
Arrival time for peak wave, t_m (sec)	=	2.28
Empirical ratio, K	=	0.098
Empirical time shift, T (sec)	=	0.04
$\frac{R\eta_m}{R_c^2}$	=	0.082

SHOT 28

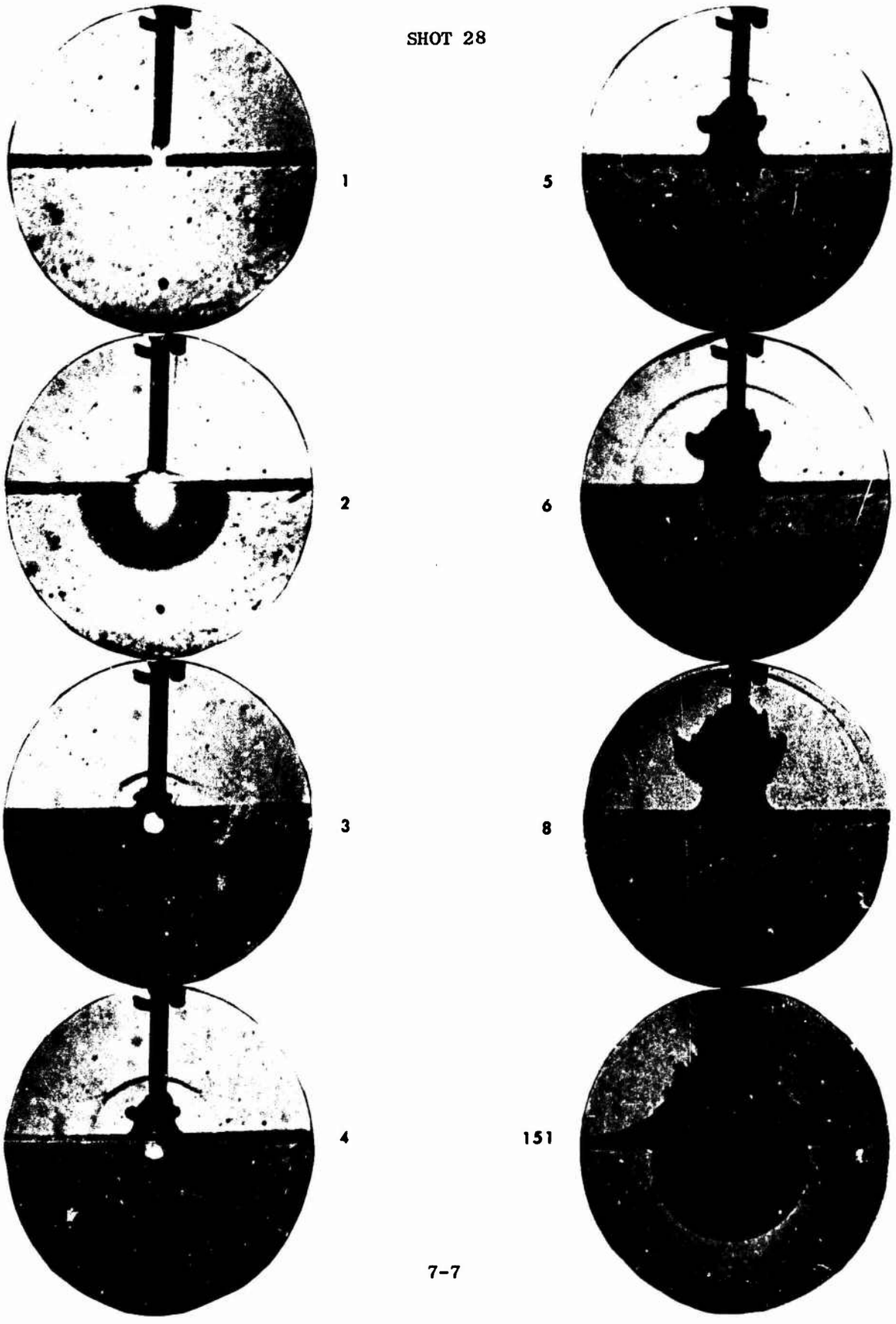

Fig. 3c, Shot No. 10, Code No. 0212691

Framing interval, (μsec)	=	40.4
Wire length (mm)	=	4.0
Wire resistance (Ω)	=	0.83
Water depth, d_w (in.)	=	36
Shot depth, d (in.)	=	1.0
Expanded cavity radius, R_c (in.)	=	2.08
Expanded cavity time, t_c (sec)	=	0.0043
Wave gage range, R (in.)	=	18
Peak wave height, η_m (in.)	=	0.030
Arrival time for peak wave, t_m (sec)	=	2.00
Empirical ratio, K	=	0.155
Empirical time shift, T (sec)	=	-0.17
$\frac{R\eta_m}{R_c^2}$	=	0.125

SHOT 10

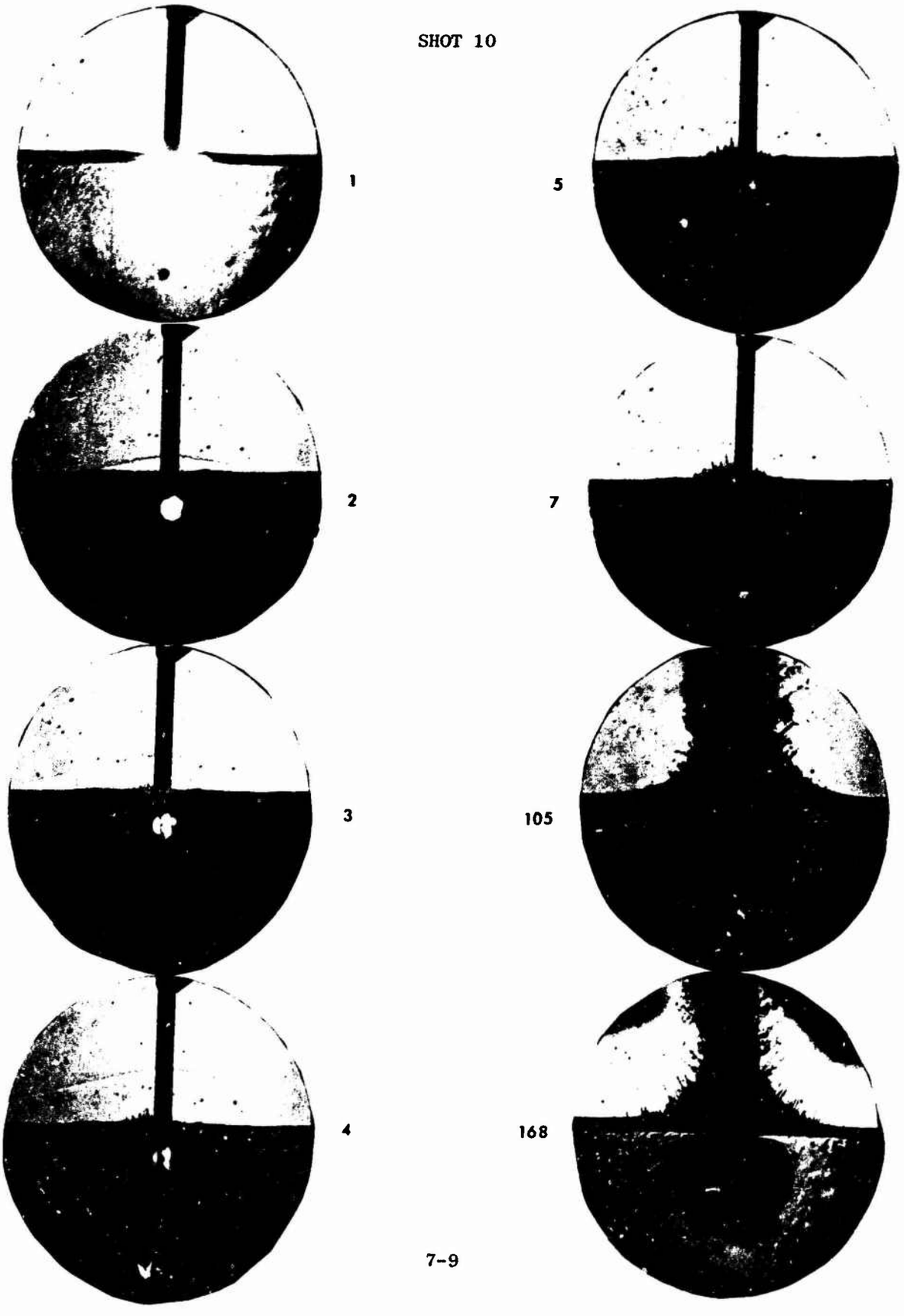

Fig. 3d, Shot No. 9, Code No. 0211691

Framing interval, (μsec)	=	40.4
Wire length (mm)	=	4.5
Wire resistance (Ω)	=	0.95
Water depth, d_w (in.)	=	36
Shot depth, d (in.)	=	2.35
Expanded cavity radius, R_c (in.)	=	2.27
Expanded cavity time, t_c (sec)	=	0.0046
Wave gage range, R (in.)	=	18
Peak wave height, η_m (in.)	=	0.045
Arrival time for peak wave, t_m (sec)	=	2.04
Empirical ratio, K	=	0.177
Empirical time shift, T (sec)	=	-0.13
$\frac{R\eta_m}{R_c^2}$	=	0.157

SHOT 9

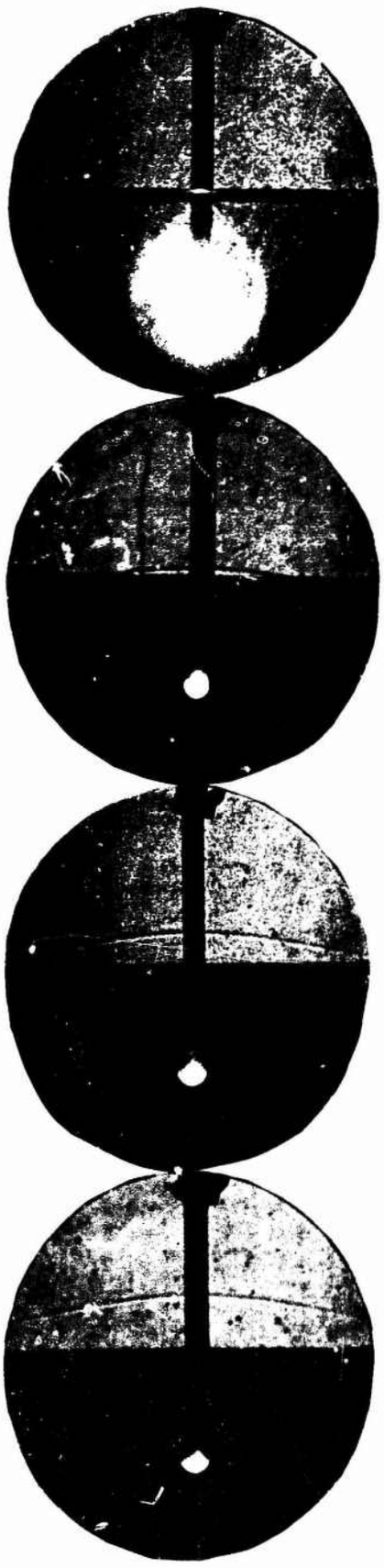

1

2

3

4

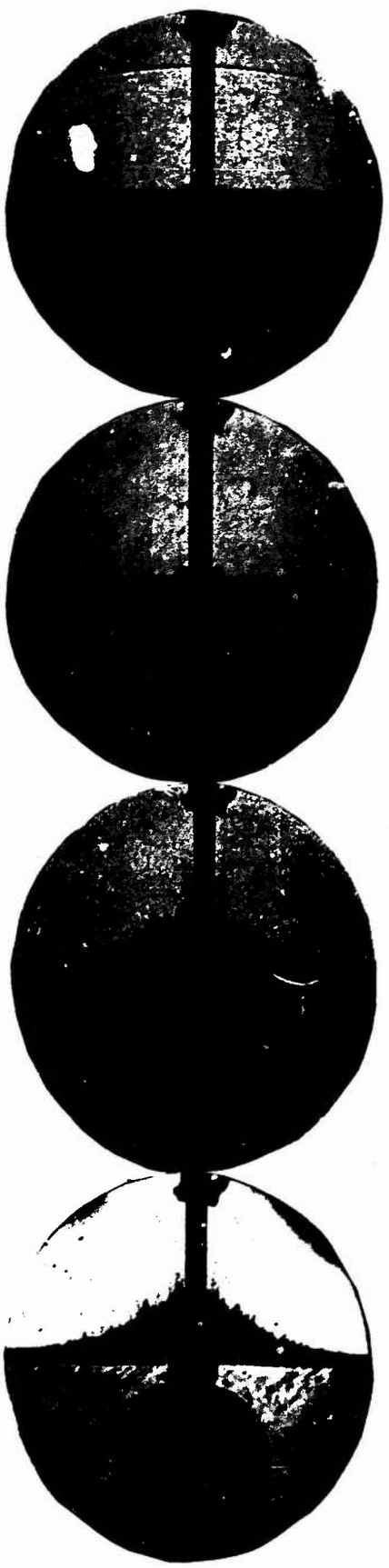

7

11

112

146

Fig. 3e, Shot No. 31, Code No. 0311692

Framing interval, (μsec)	=	40.5
Wire length (mm)	=	3.0
Wire resistance (Ω)	=	0.95
Water depth, d_w (in.)	=	36
Shot depth, d (in.)	=	3.94
Expanded cavity radius, R_c (in.)	=	2.07
Expanded cavity time, t_c (sec)	-	-
Wave gage range, R (in.)	=	19
Peak wave height, η_m (in.)	=	0.020
Arrival time for peak wave, t_m (sec)	=	-
Empirical Ratio, K	=	-
Empirical time shift, T (sec)	=	-
$\frac{R\eta_m}{R_c^2}$	=	0.089

SHOT 31

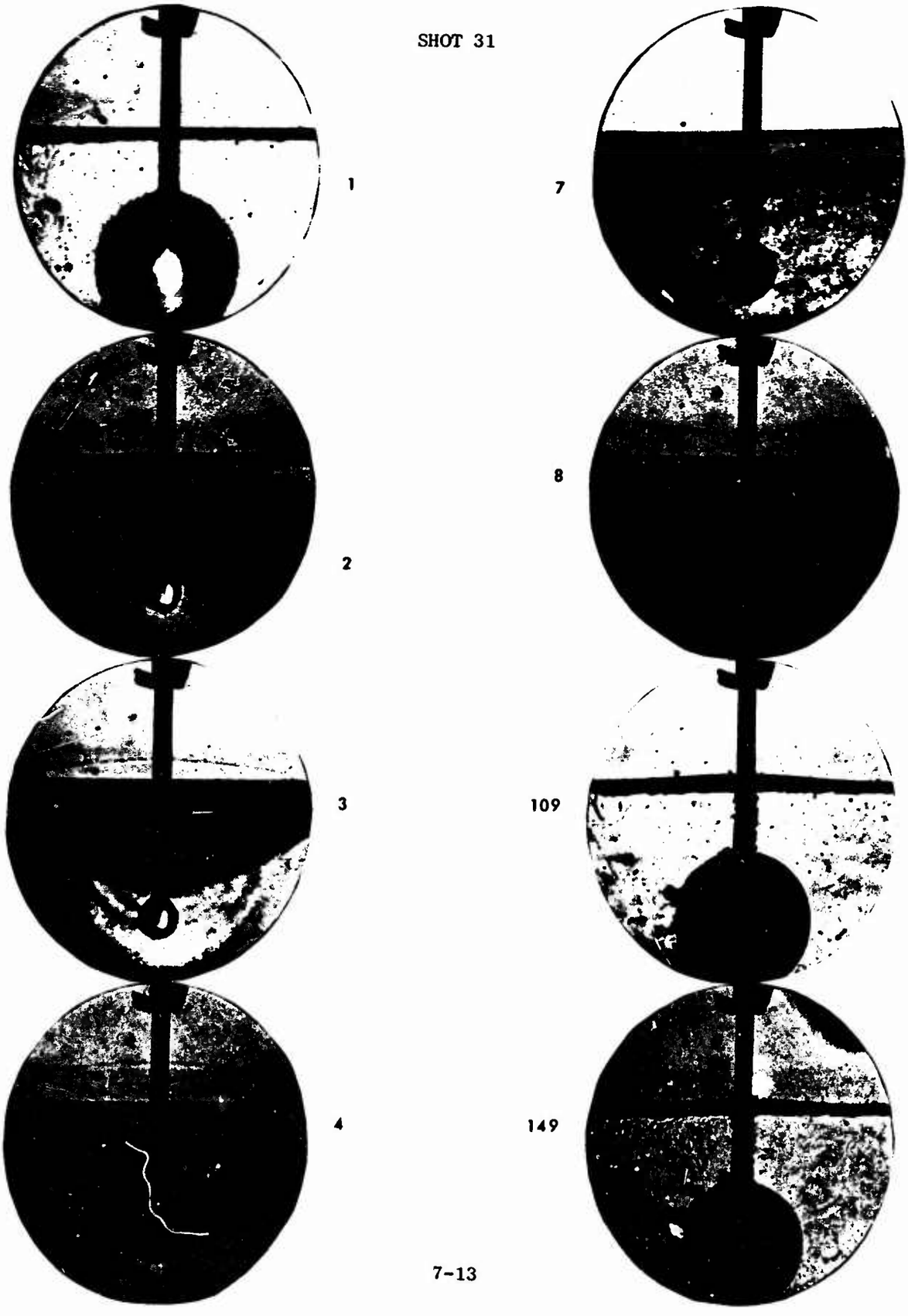

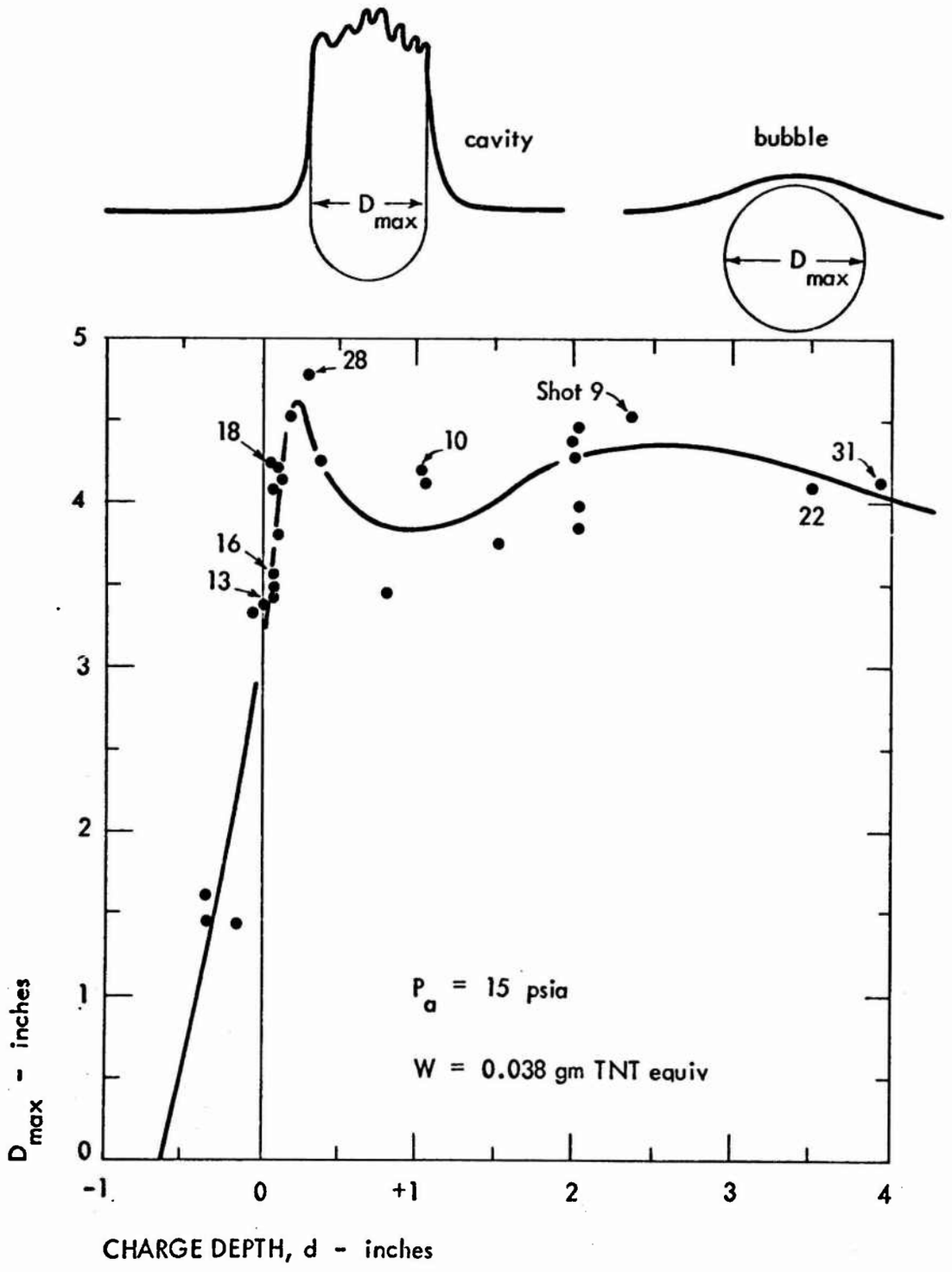

Fig. 4. Maximum Diameter of Cavities and Bubbles from Wires Exploded in Deep Water

[redacted] 679-6

SHOT NUMBER	CHARGE DEPTH, d (in.)	SWEEP RATE (μsec/cm)
28	0.30	50
10	1.00	50
9	2.35	50
31	3.94	100

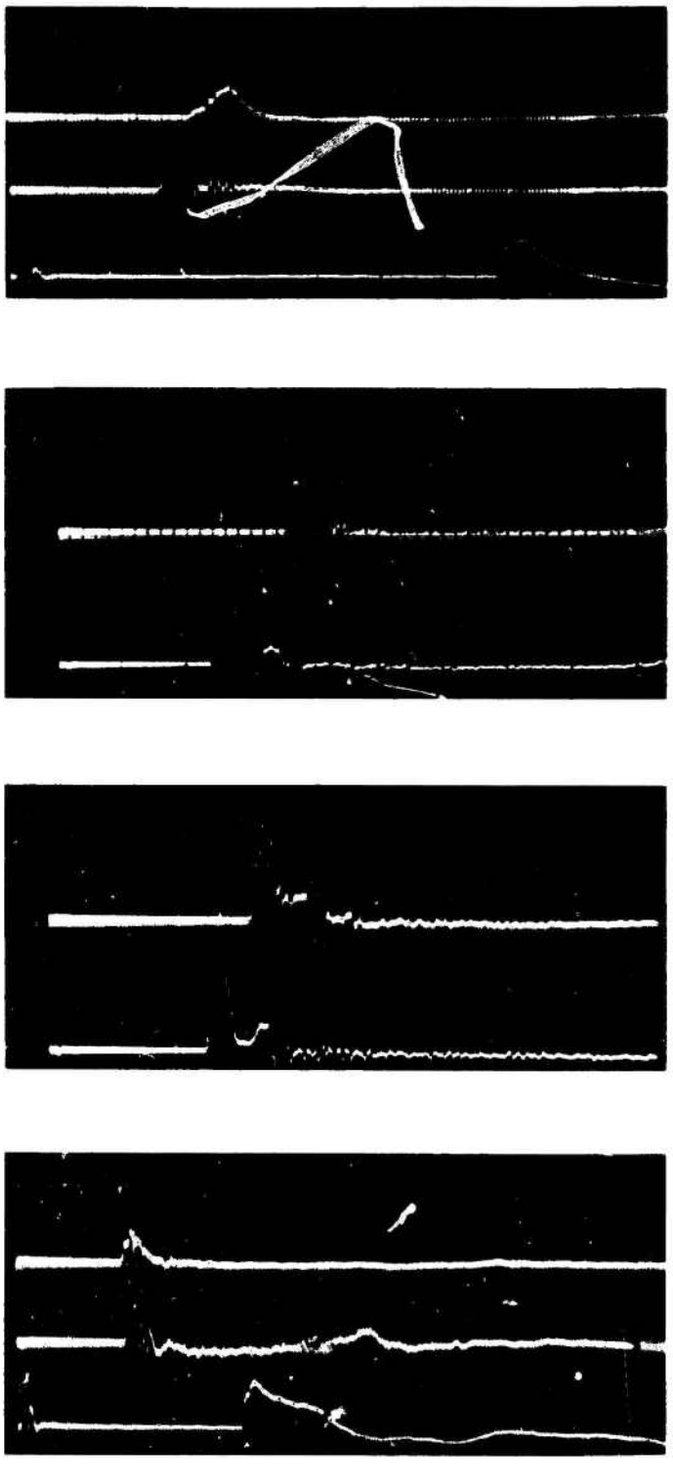

NOTE: See Table 3 for additional data.

Fig. 5. Water Shock Wave Pressure– Time Histories

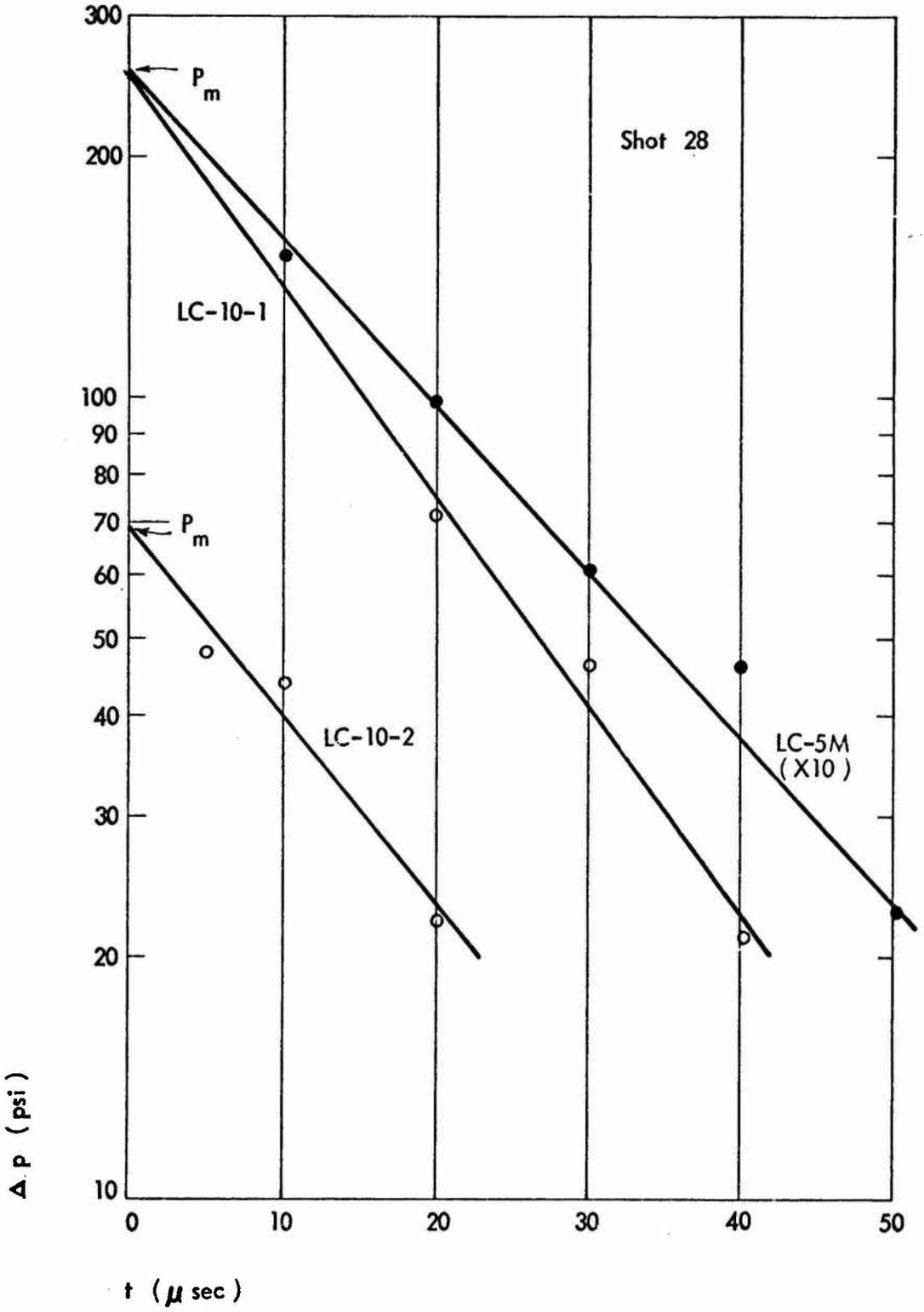

Fig. 6. Method for Extrapolating to Time of Arrival to Determine Peak Pressure

Fig. 7. Surface Wave Trains for Exploding Wires at Eight Depths of Burst

	Crest	Trough
Calc	□	o
Meas	×	✳

K = 0.394

T (sec) = -0.07

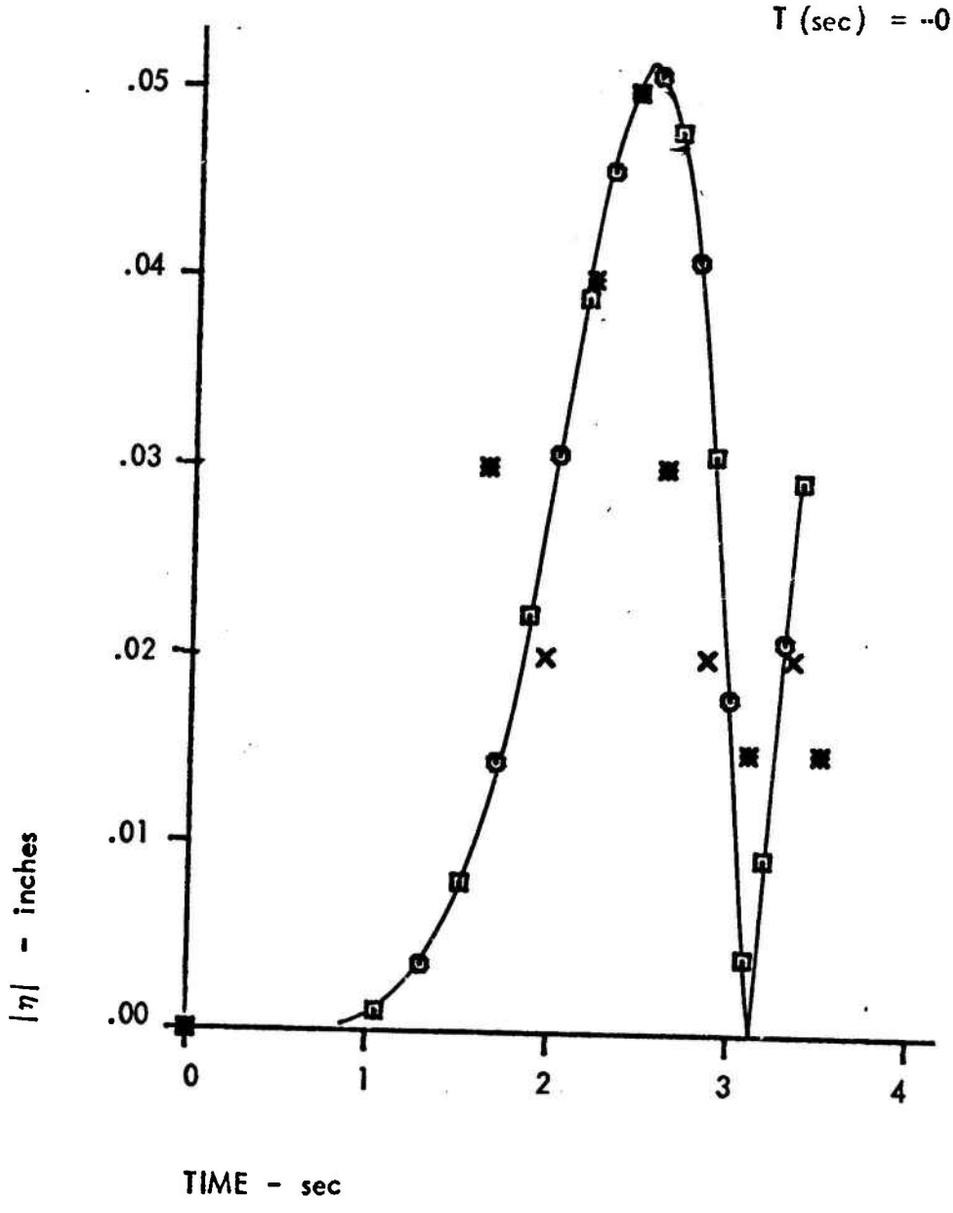

Fig. 7a. Shot 21, d = 0 in.

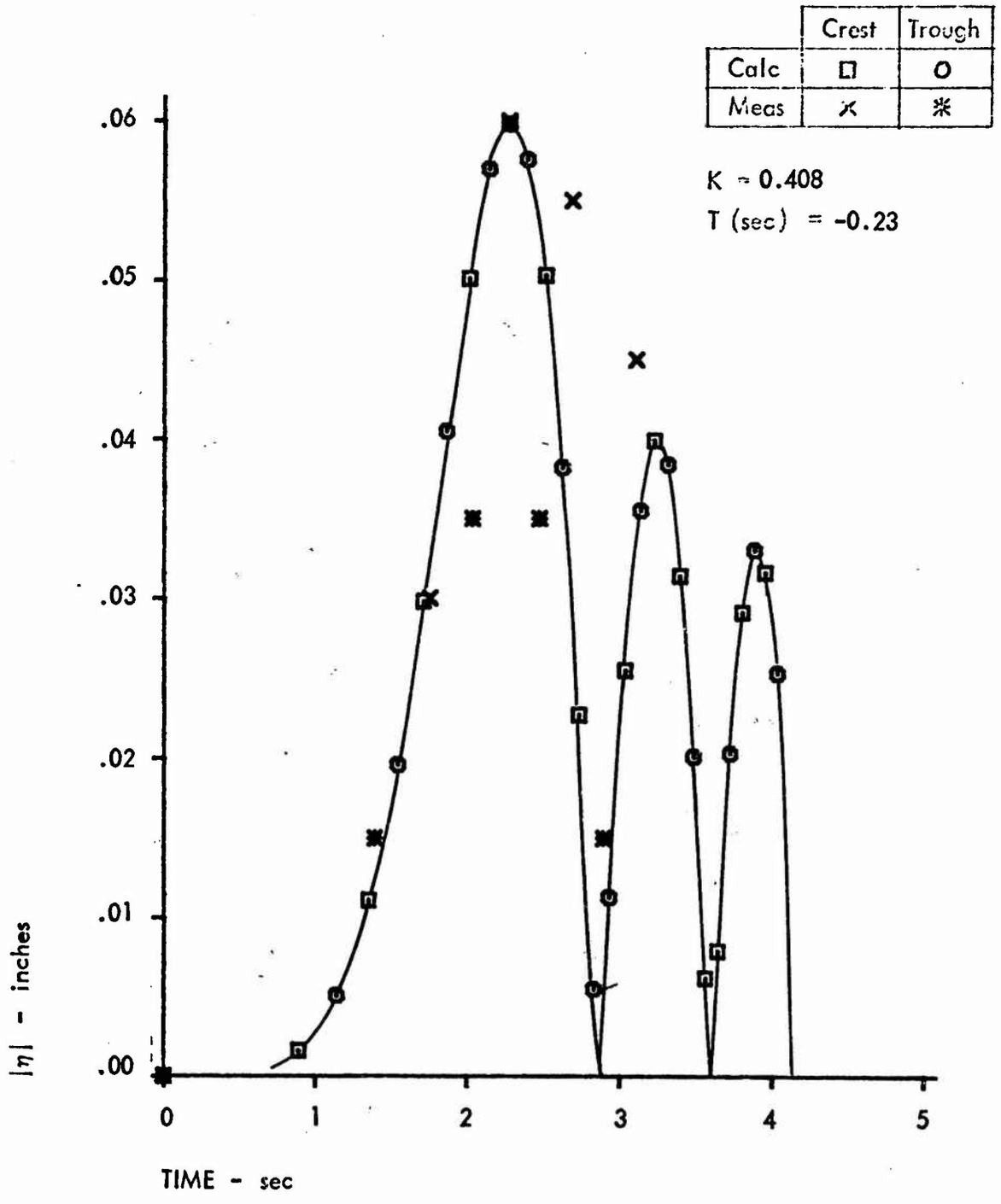

Fig. 7b. Shot 16, d = 0.06 in.

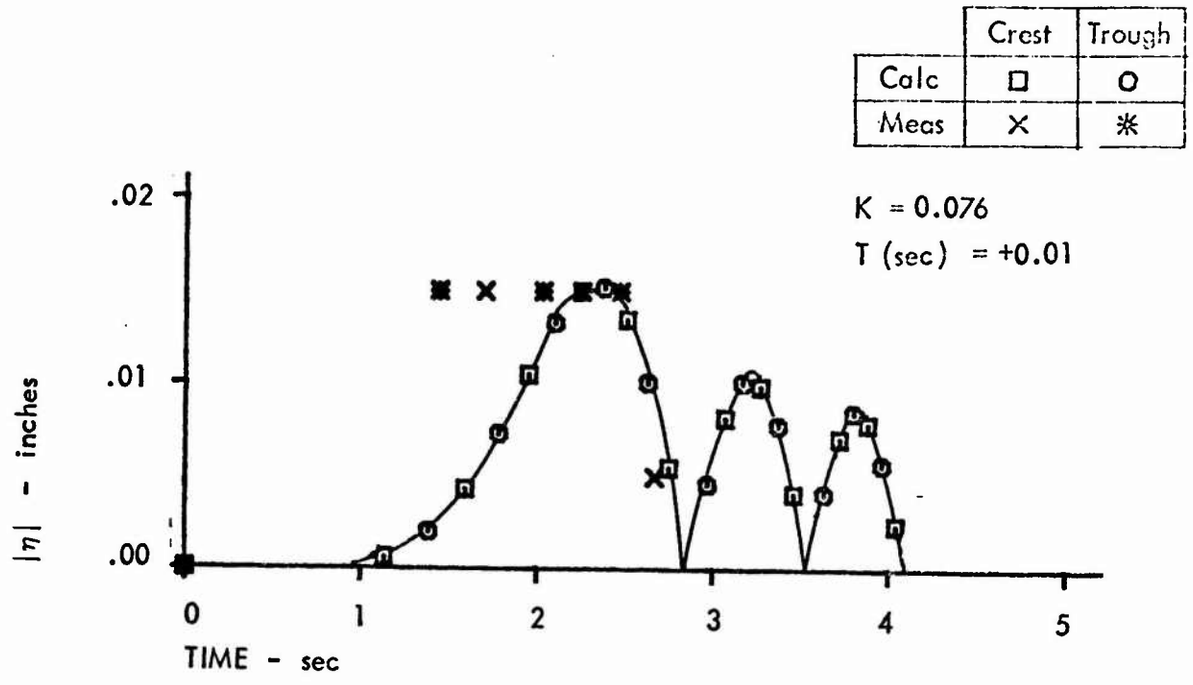

Fig. 7c. Shot 18, d = 0.09 in.

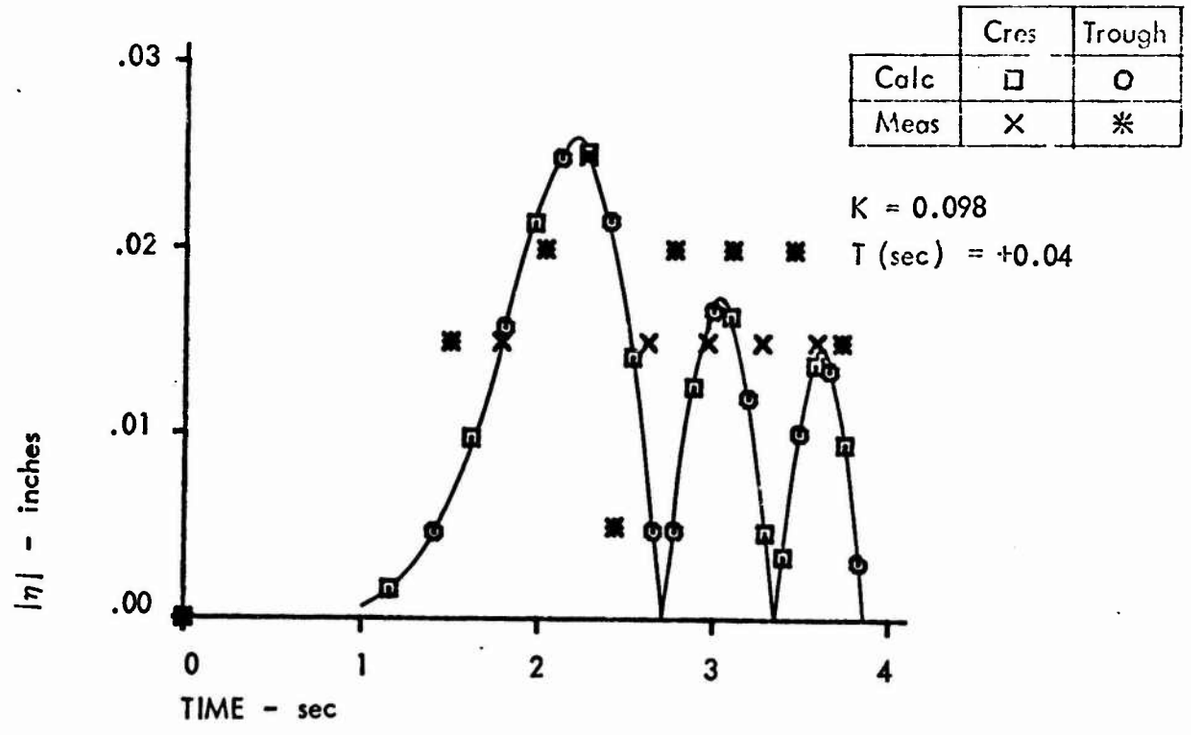

Fig. 7d. Shot 28, d = 0.30 in.

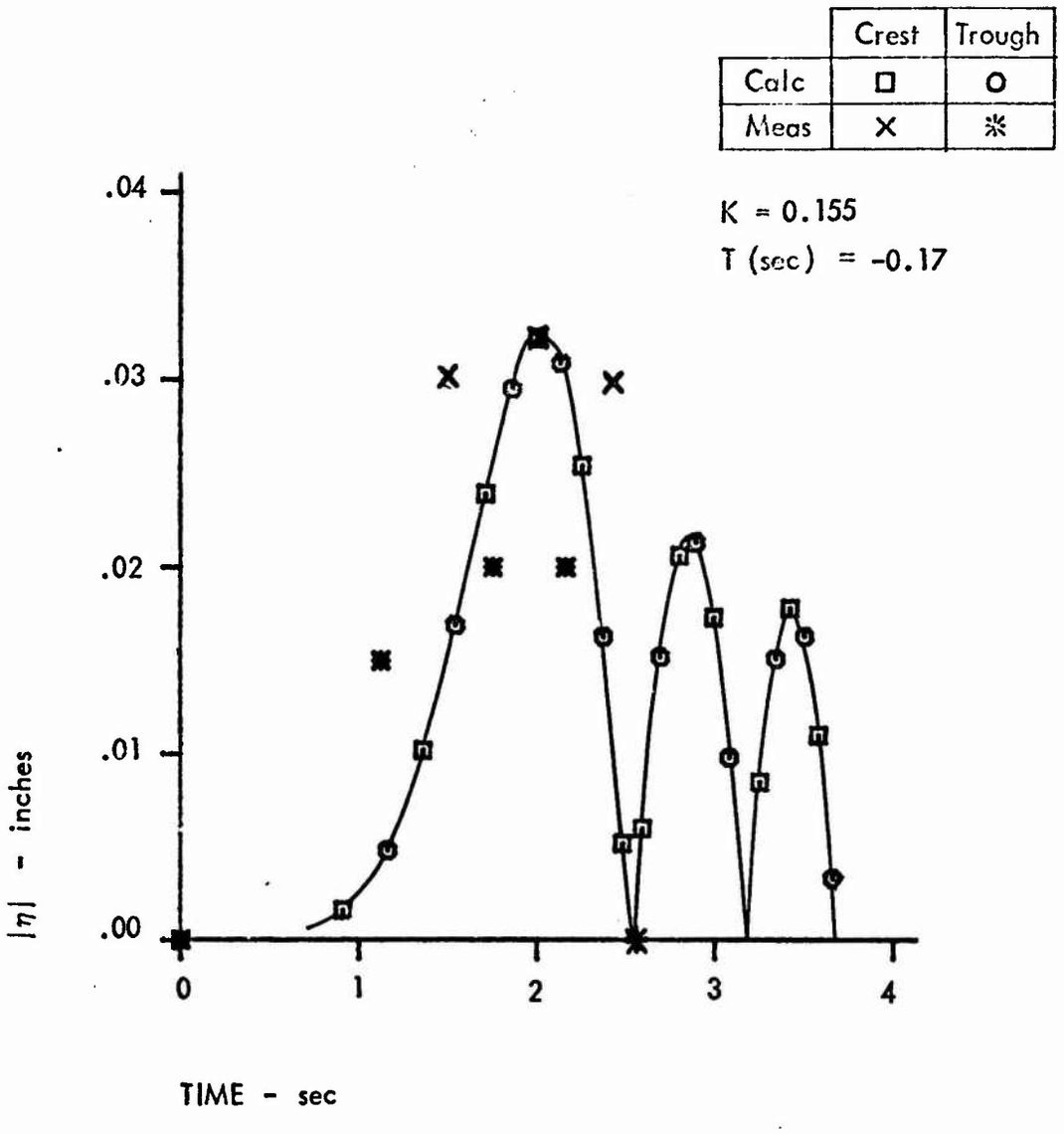

Fig. 7e. Shot 10, d = 1.0 in.

	Crest	Trough
Calc	□	o
Meas	×	✳

K = 0.222

T (sec) = -0.01

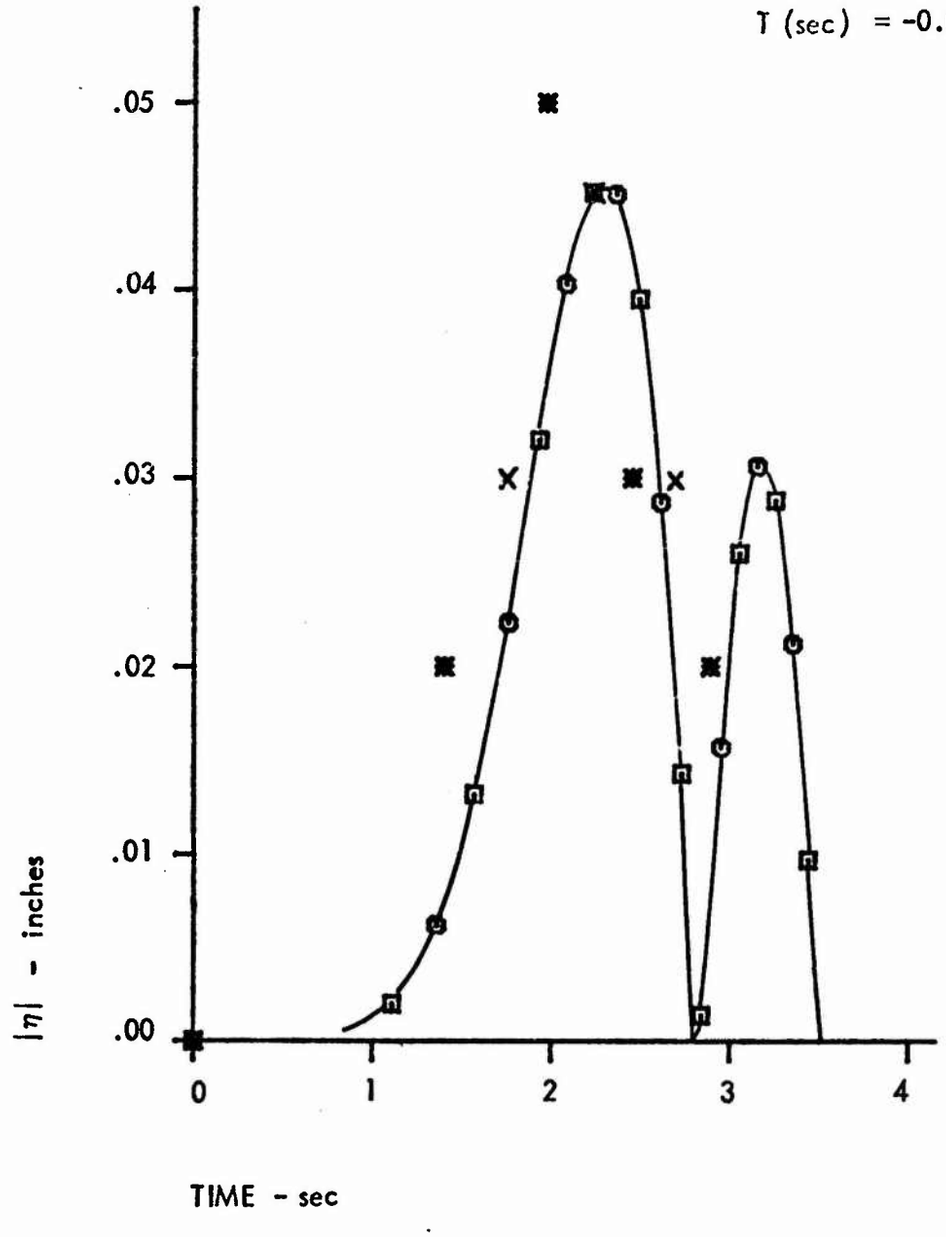

Fig. 7f. Shot 25, d = 2.0 in.

	Crest	Trough
Calc	□	O
Meas	×	✳

K = 0.177

T (sec) = -0.13

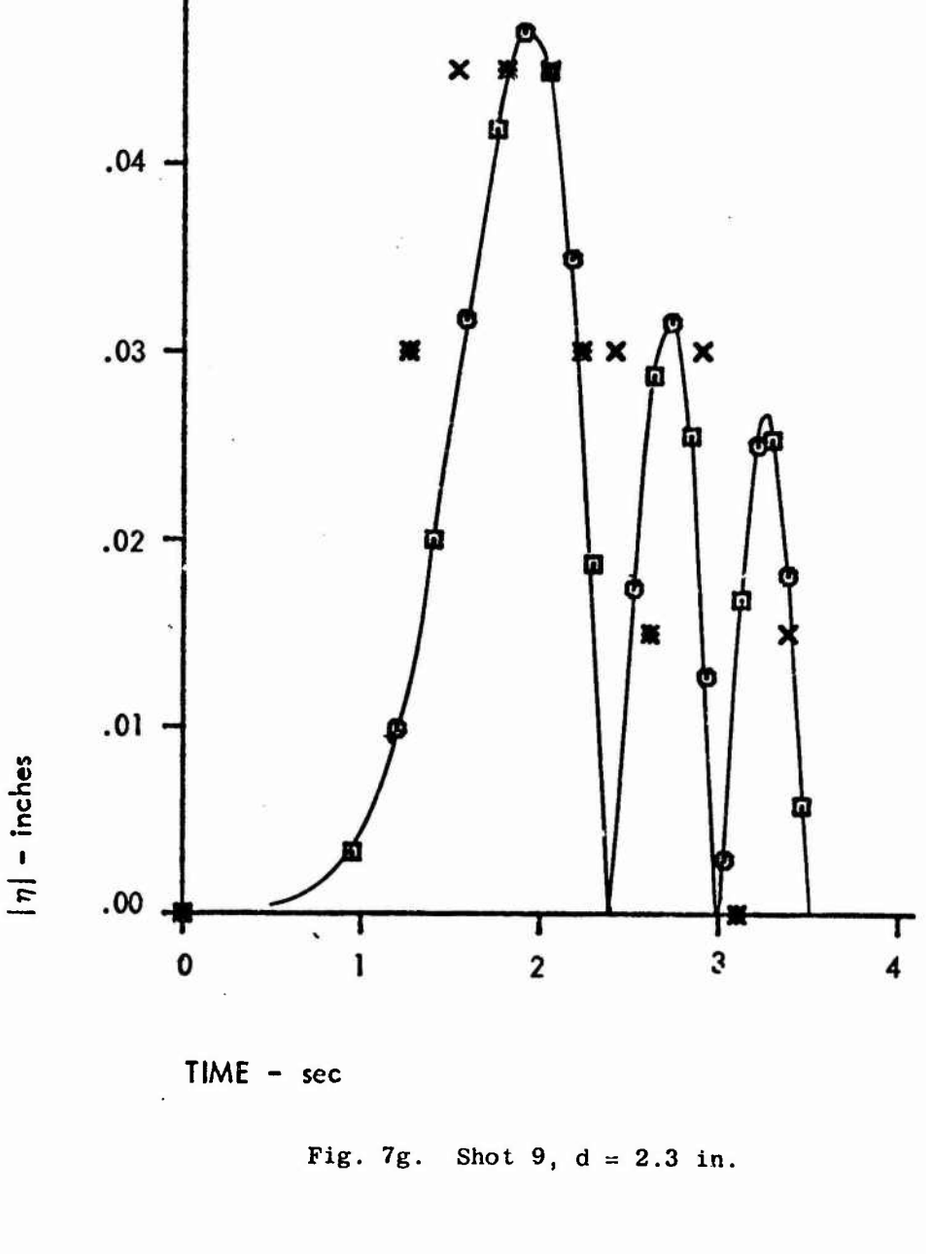

Fig. 7g. Shot 9, d = 2.3 in.

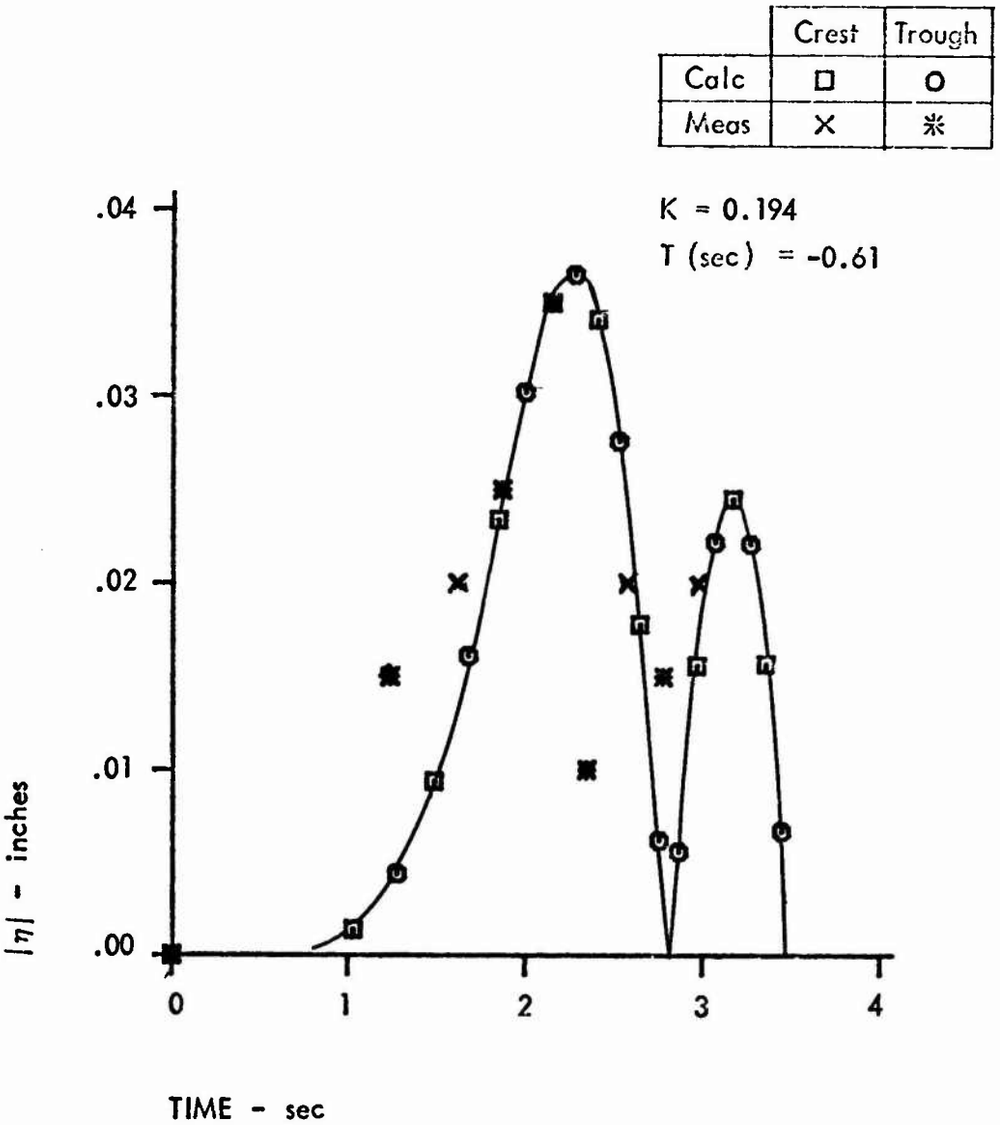

Fig. 7h. Shot 22, d = 3.4 in.

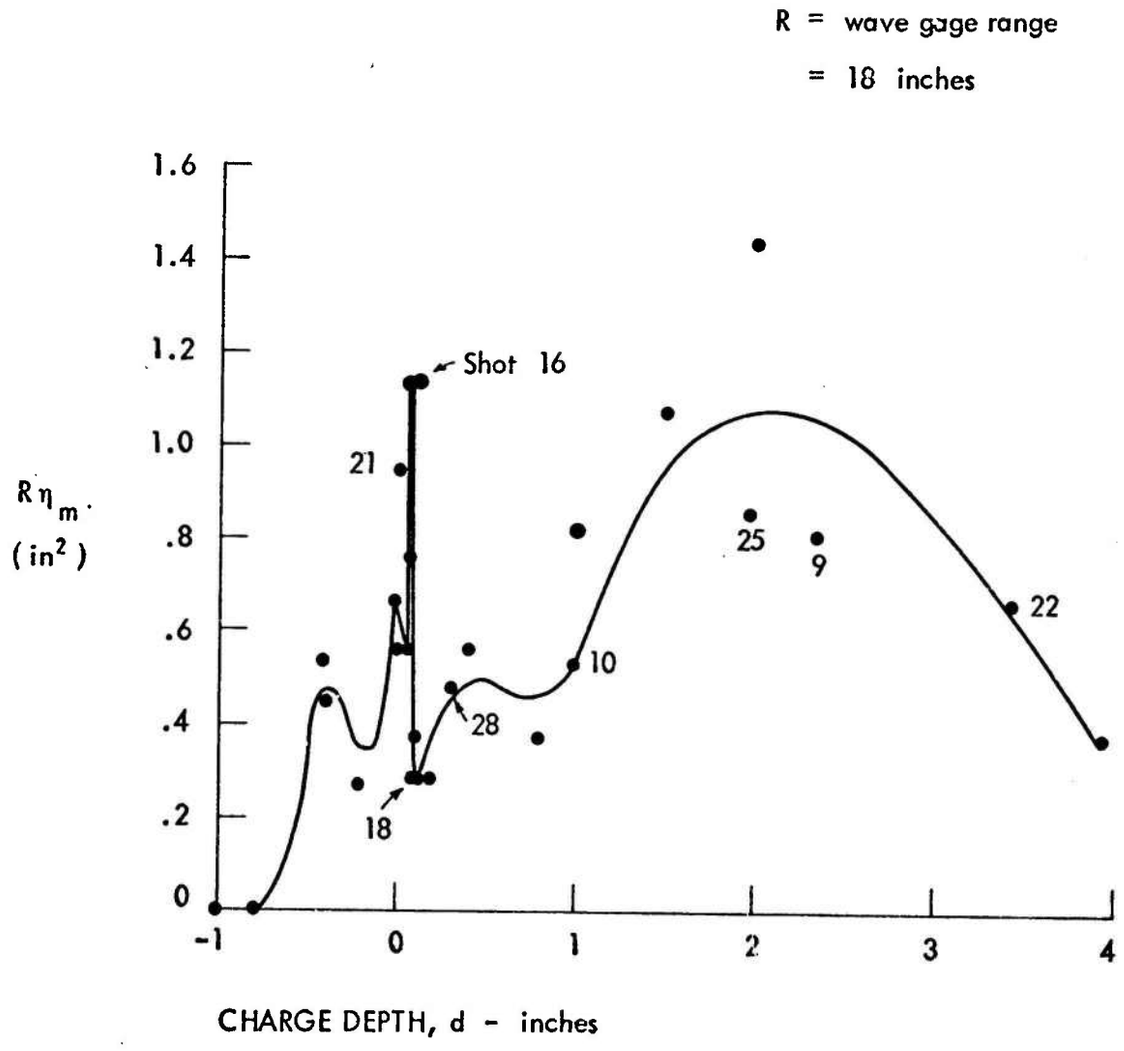

Fig. 8. Measured Values of Peak Wave Height η_m versus Charge Depth d

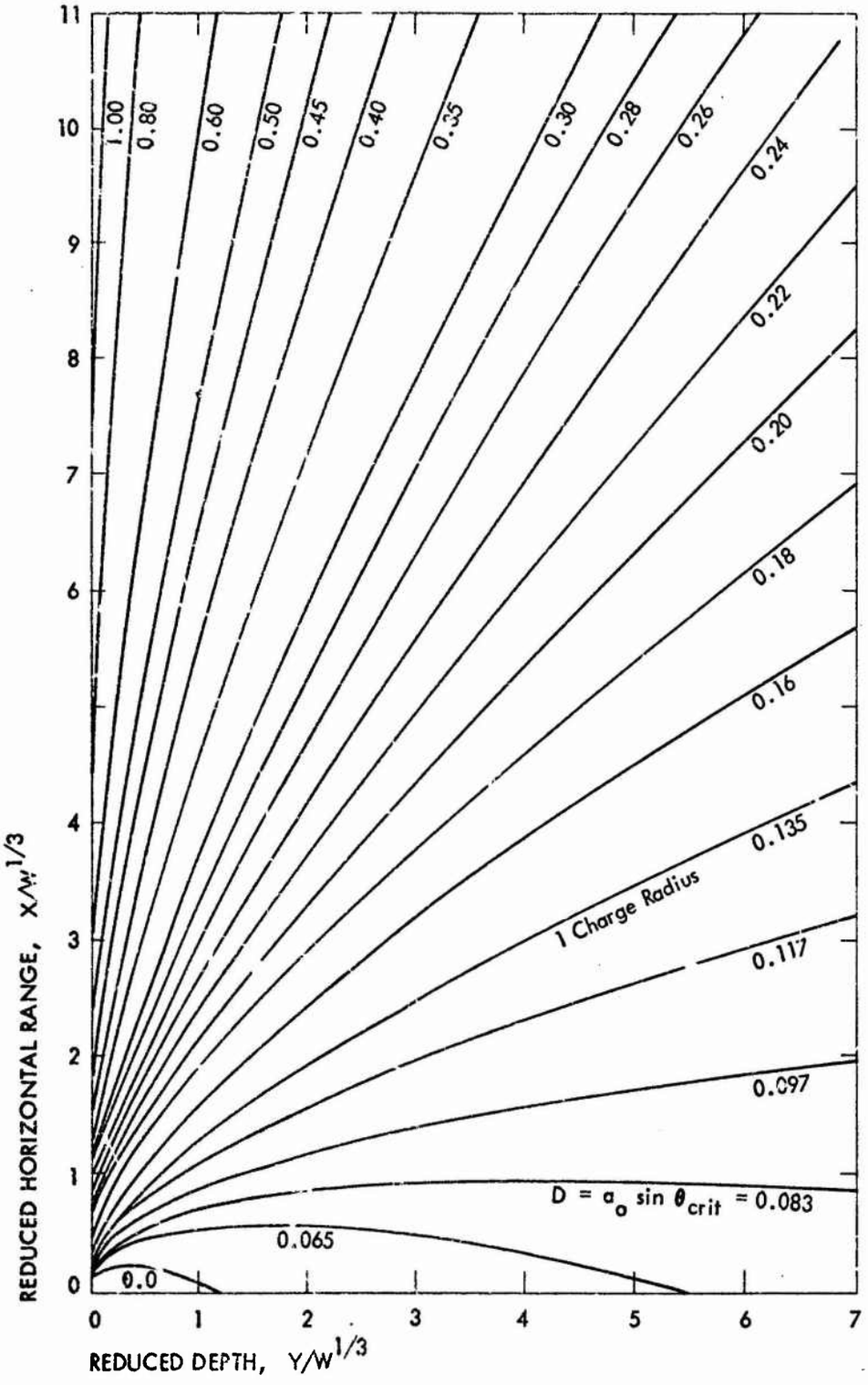

Fig. 9. Lower Boundary of Region of Anomolous Surface Reflection for TNT Charges. The parameter is the reduced depth of explosion, $D/W^{1/3}$

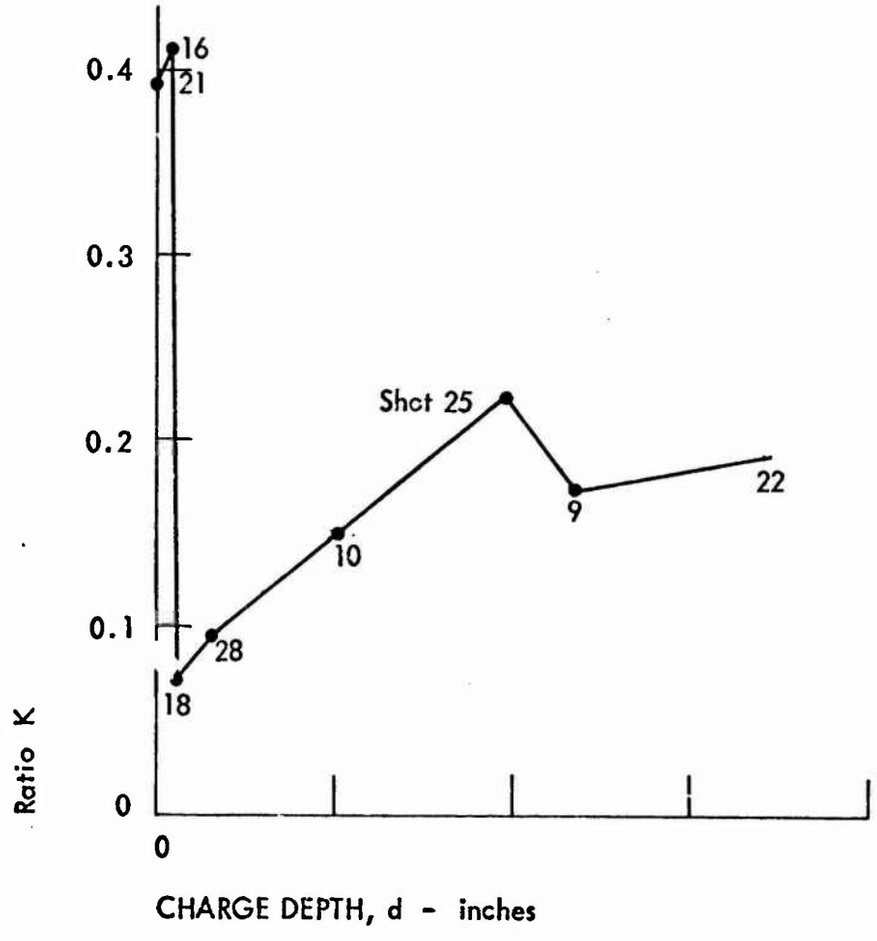

Fig. 10. Ratio of Measured/Theoretical Peak Wave Height, K, versus Charge Depth, d

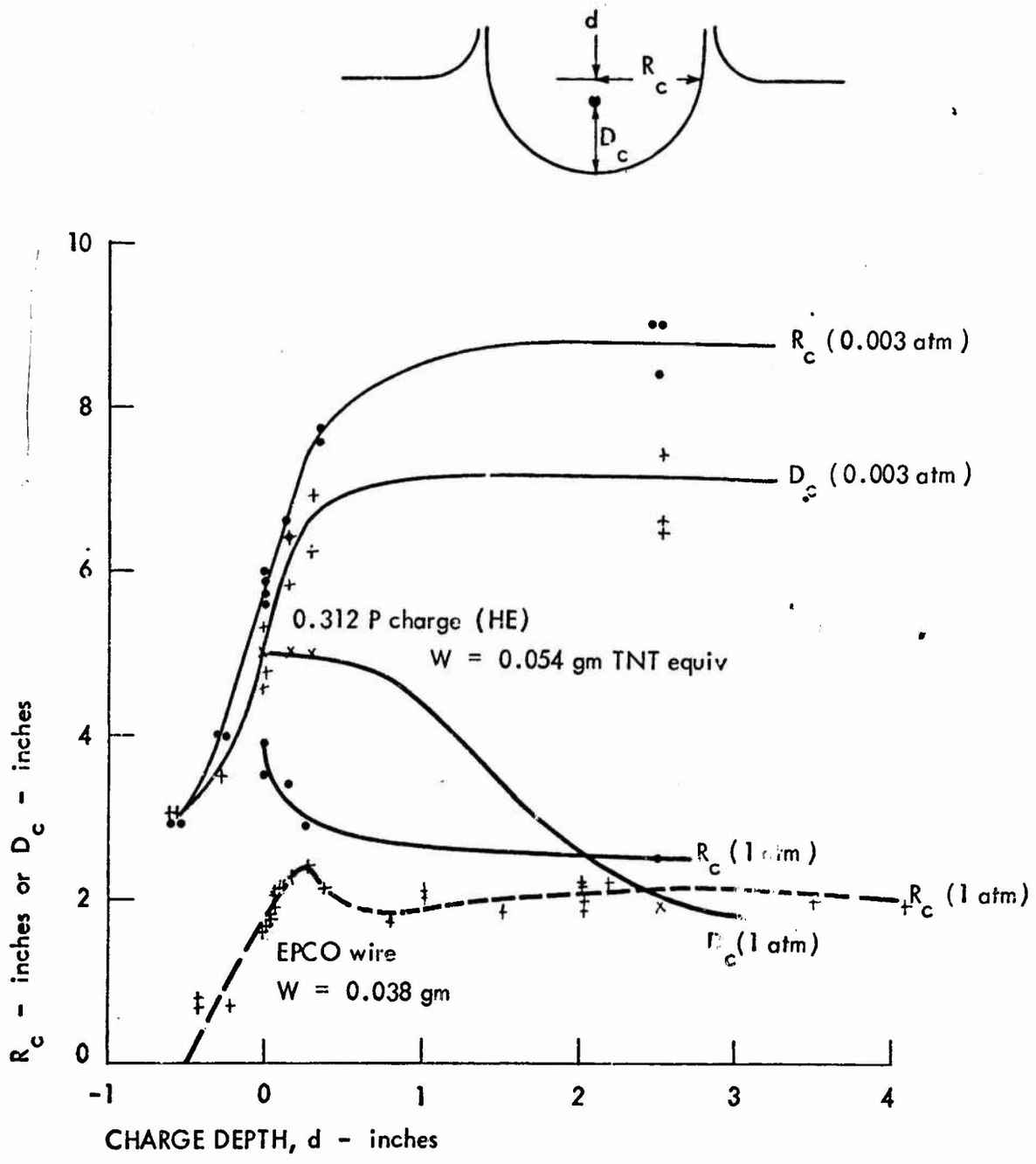

Fig. 11. Comparison of Expanded Cavities from a Small HE Charge and an Exploding Wire versus Charge Depth

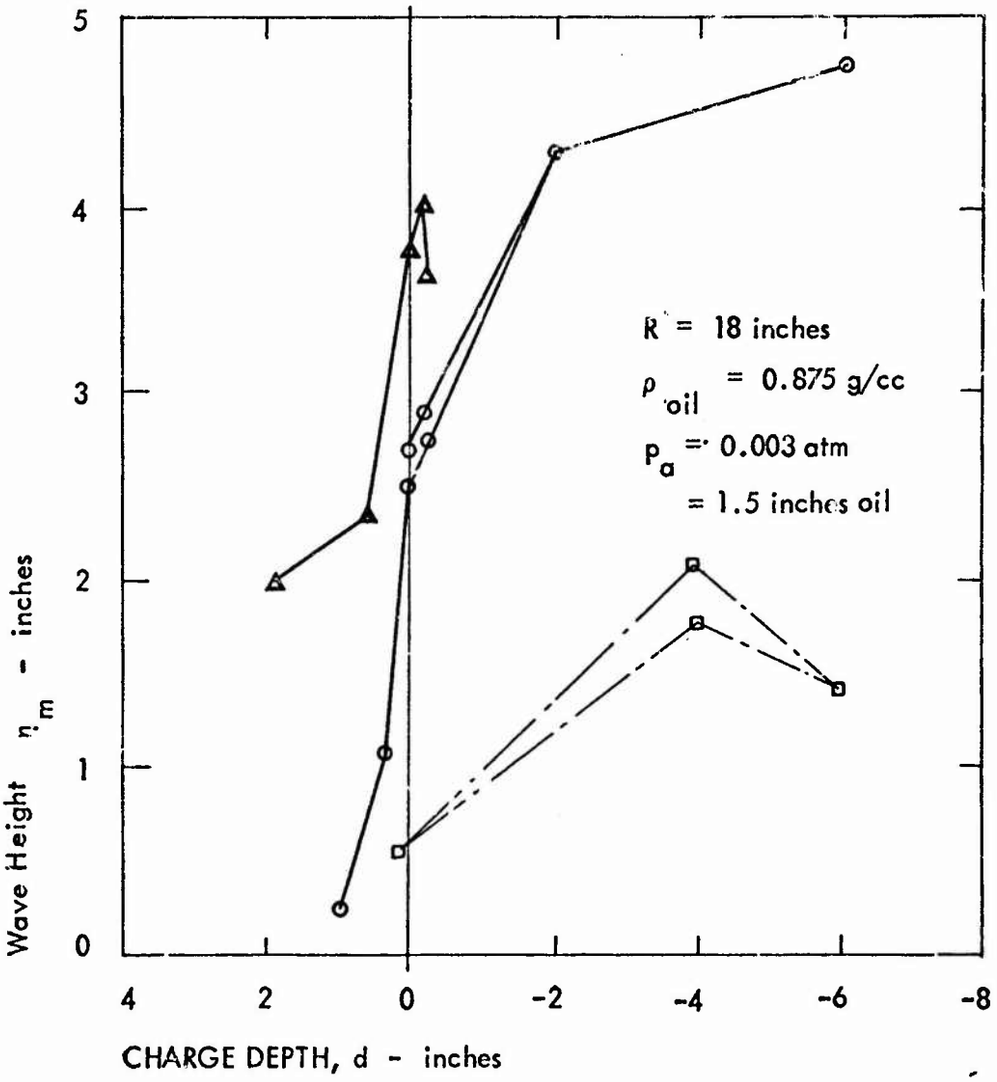

NOTES :

- o 0.312 P charge, W = 0.054 gm TNT equiv
- □ 0.312 A charge, W = 0.17 gm TNT equiv
- △ 0.60 A charge, W = 1.57 gm TNT equiv

Fig. 12. Second Wave Height versus Charge Depth for Three Charge Sizes in Deep Fluid

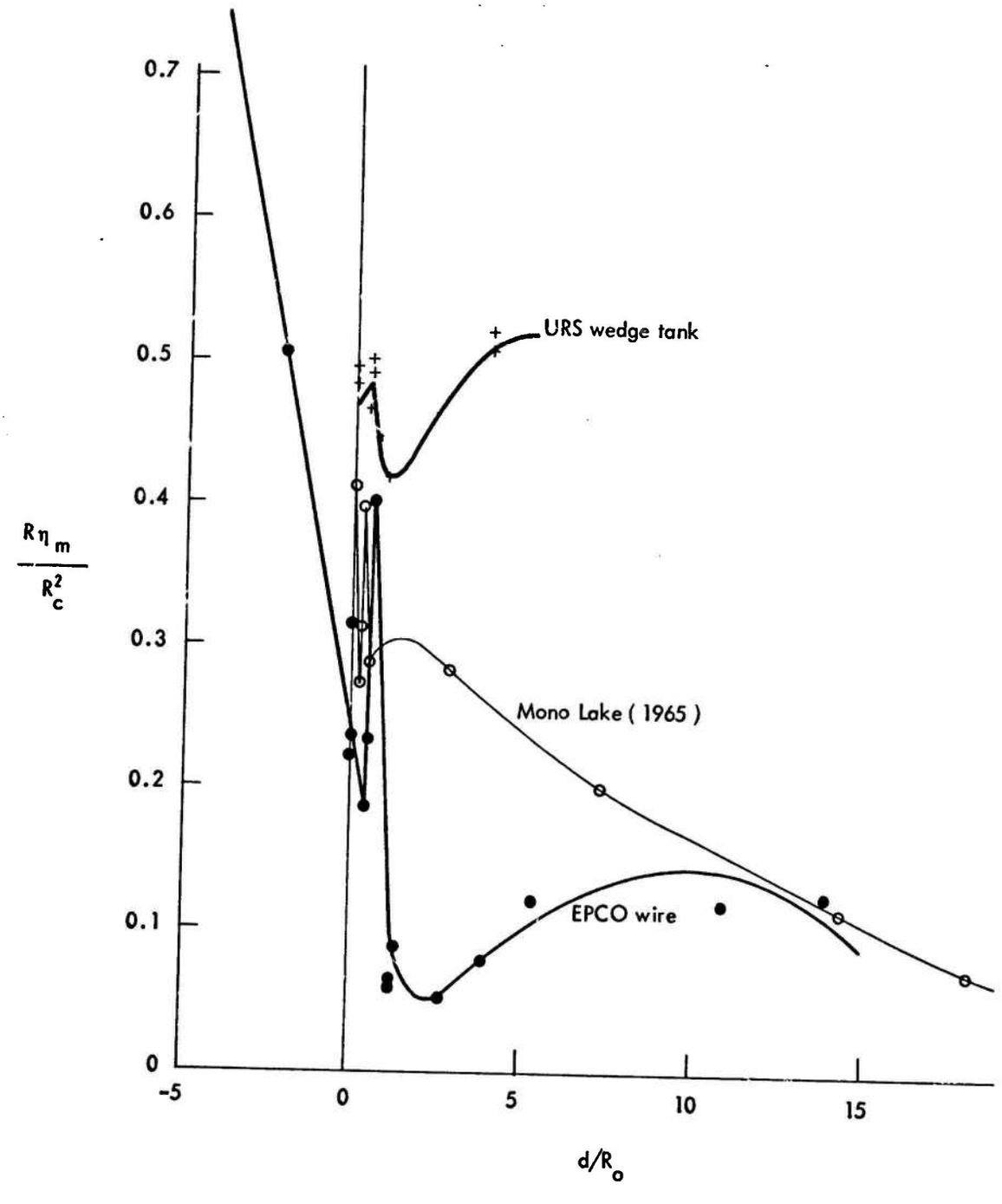

Fig. 13. Dimensionless Ratios for Peak Wave Height versus Depth of Burst

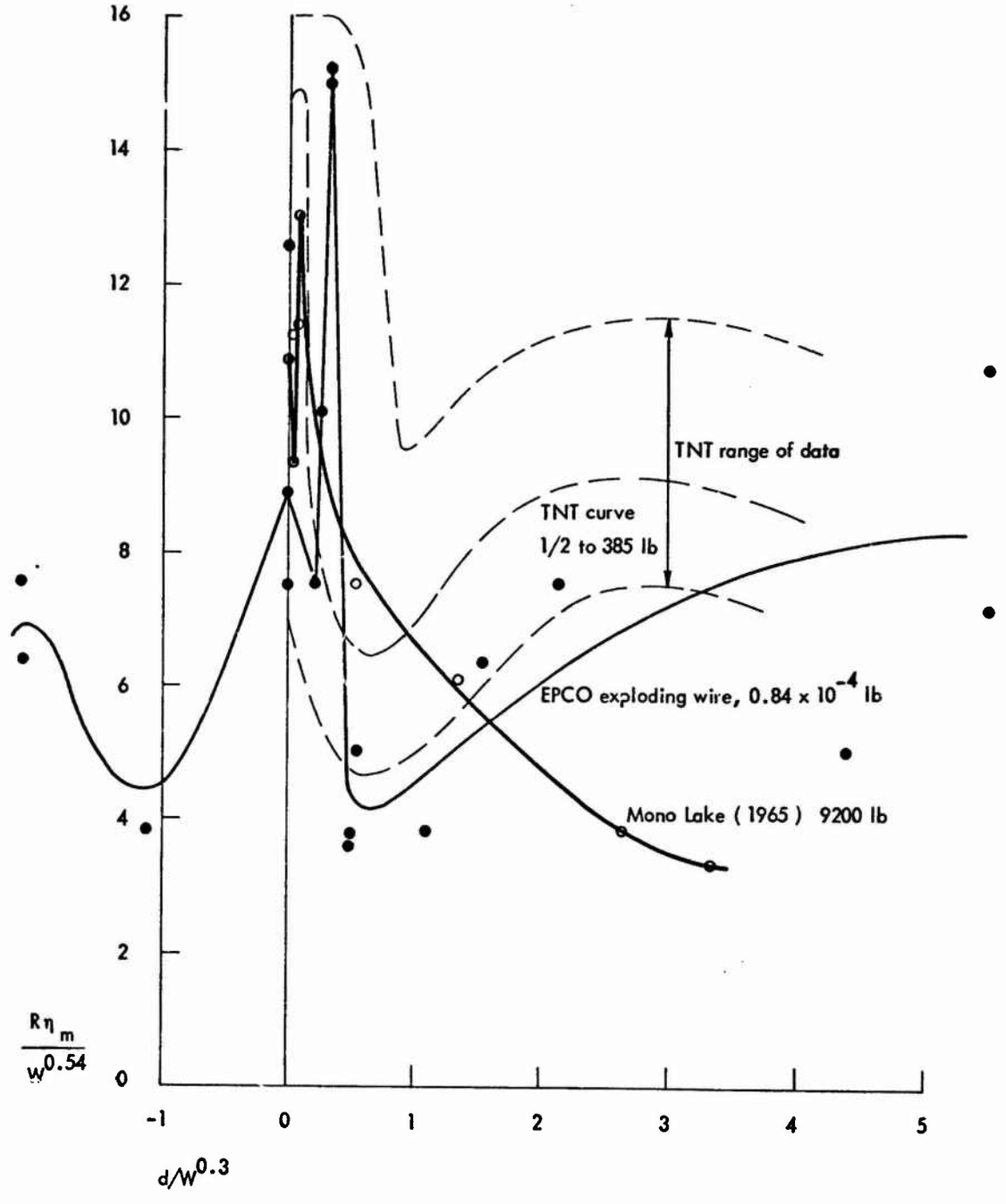

Fig. 14. Reduced Values of Peak Wave Height versus Charge Depth

SHOT 16

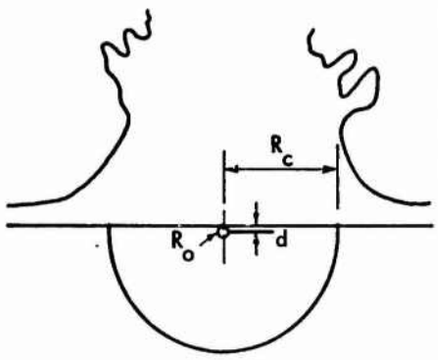

d (in.)	R_c (m)	t_c (sec.)	η_m (in.)	$\frac{R\tau_{i_m}}{R_c^2}$
0.06	1.78	0.007	0.060	0.399

SHOT 18

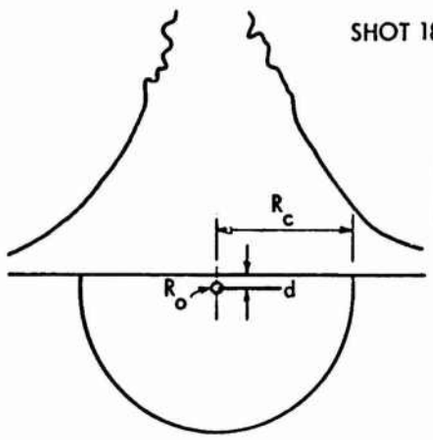

0.09	2.11	0.004	0.015	0.061

SHOT 28

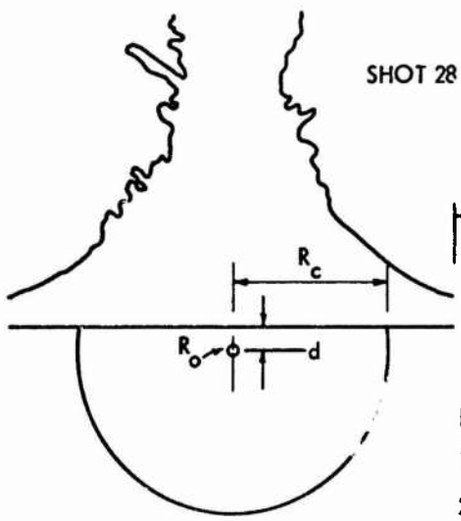

0.295	2.39	0.007	0.025	0.079

NOTES:

1) All shots under normal pressure

2) Equivalent TNT charge radius, R_o = 0.072 inches

Fig. 15. Water Columns and Cavities for Near-Surface Bursts

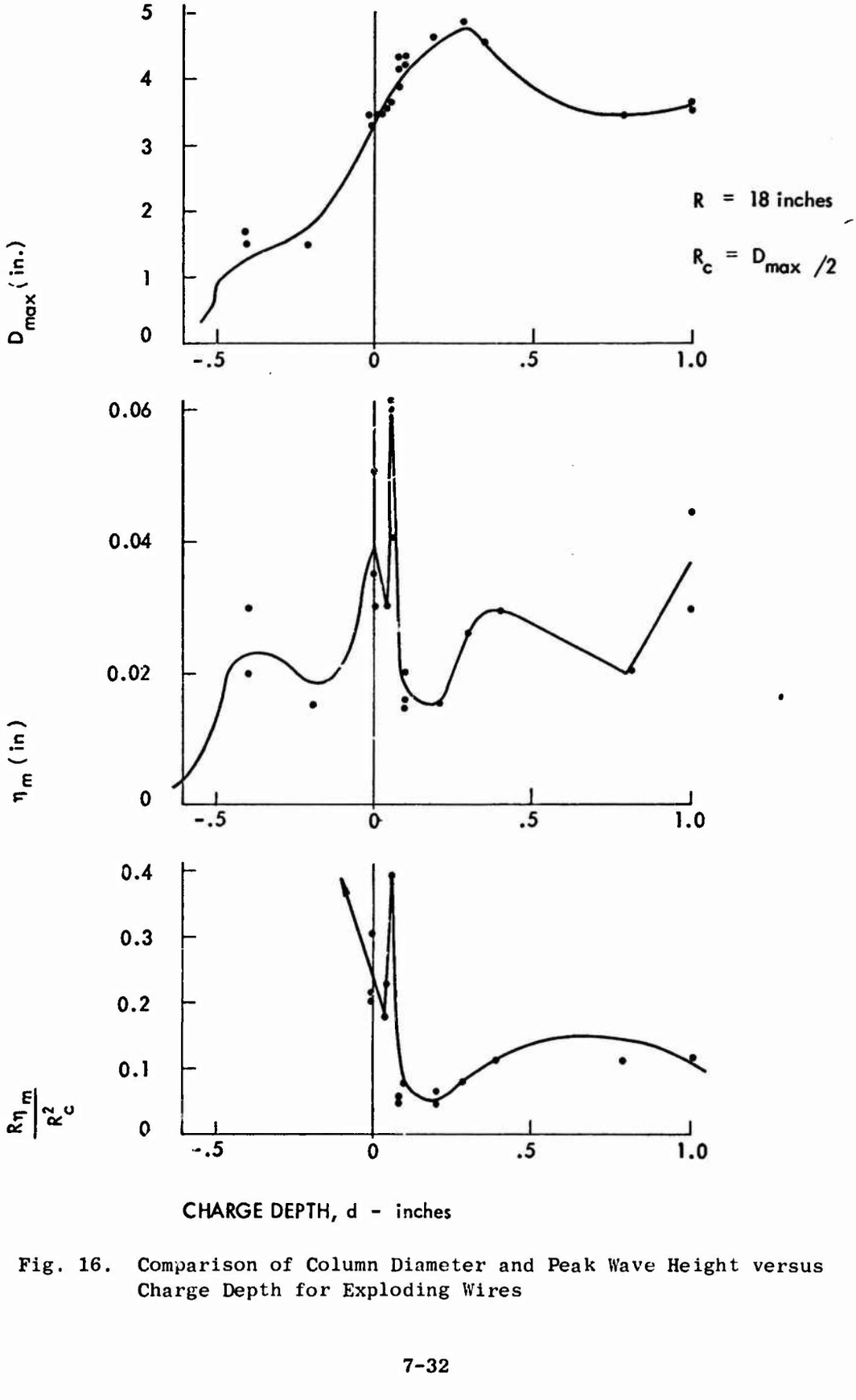

Fig. 16. Comparison of Column Diameter and Peak Wave Height versus Charge Depth for Exploding Wires

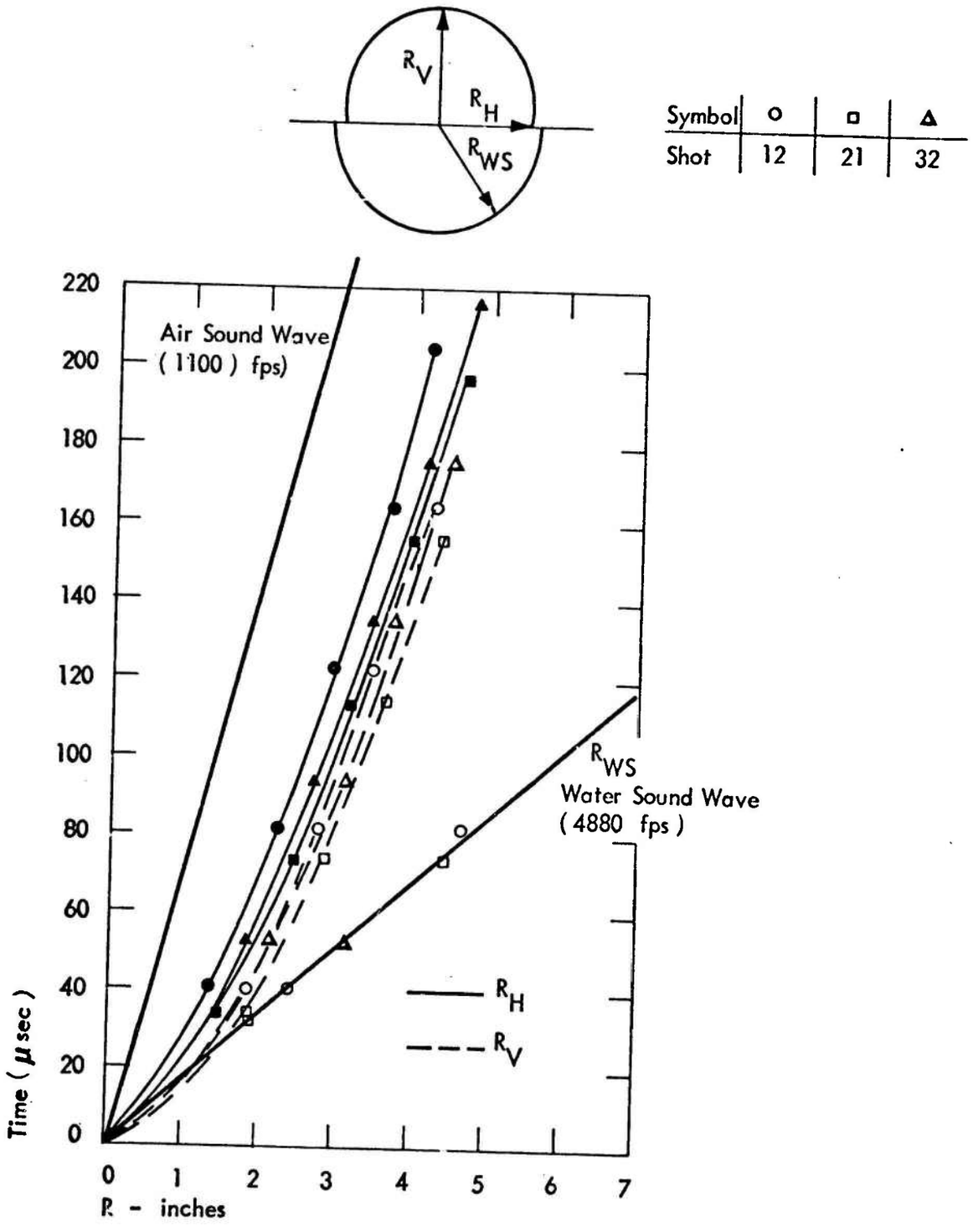

Fig. 17. Radii of Air and Water Shock Wave Fronts versus Time for Zero Charge Depth

Table 1

LISTING OF TESTS

Test No.	Code No.	Charge Depth, d (in.)	Wire Length (' ')	Wire Resistance Ω	Cavity Record	Pressure Record	Three Complete Records	35-mm Frame Separation (μsec)
1	0131691	2.50	3.2	0.77	No	Yes	No	40.1
2	0131692	2.00	3.3	0.81	Yes	Yes	No	40.1
3	0131693	1.50	3.4	0.92	Yes	Yes	No	40.1
4	0131694	1.00	3.5	0.98	Yes	Yes	No	40.1
5	0203691	1.50	3.7	1.01	Yes	Yes	No	40.1
6	0206691	1.50	3.0	0.94	Yes	Yes	Yes	40.1
7	0206693	2.00	2.6	0.72	No	Yes	No	--
8	0207691	2.00	2.6	0.72	Yes	Yes	Yes	40.4
9	0211691	2.35	4.5	0.95	Yes	Yes	Yes	40.4
10	0212691	1.00	4.0	0.83	Yes	Yes	Yes	40.4
11	0218691	1.00	4.0	0.80	No	No	No	40.7
12	0218692	0	3.0	0.80	Yes	Yes	Yes	40.7
13	0218693	0.04	2.4	0.69	Yes	Yes	Yes	40.5
14	0219691	0.05	3.5	0.80	Yes	Yes	Yes	40.6
15	0219692	0.06	3.5	0.80	No	Yes	No	40.5
16	0224691	0.06	3.0	0.84	Yes	Yes	Yes	40.5
17	0225691	0.09	2.8	0.78	Yes	Yes	No	40.8
18	0227691	0.09	4.5	1.18	Yes	Yes	Yes	40.5
19	0228691	0.09	2.5	0.86	Yes	Yes	Yes	40.7
20	0228692	0.10	3.5	0.96	Yes	Yes	Yes	40.5
21	0303691	0	4.5	1.17	Yes	Yes	Yes	40.5
22	0304691	3.44	2.5	0.84	Yes	Yes	Yes	40.6
23	0305691	1.97	4.0	0.99	Yes	Yes	No	40.5
24	0305692	1.97	3.8	1.08	Yes	No	No	40.5
25	0306691	1.97	2.7	0.8	Yes	Yes	Yes	40.5
26	0307691	0.788	2.3	0.72	Yes	Yes	Yes	40.6
27	0307692	0.394	2.8	0.91	Yes	Yes	Yes	40.5
28	0310691	0.295	3.6	1.12	Yes	Yes	Yes	40.5
29	0310692	0.197	3.3	1.04	Yes	Yes	Yes	40.6
30	0311691	0.098	3.0	0.96	Yes	Yes	Yes	40.6
31	0311692	3.94	3.0	0.95	Yes	Yes	Yes	40.5
32	0312691	0	3.3	0.97	Yes	Yes	Yes	40.7
33	0312692	-0.20	3.9	1.04	Yes	Yes	Yes	40.6
34	0313691	-0.39	2.8	0.90	Yes	No	No	40.6
35	0313692	-0.39	4.1	1.19	Yes	Yes	Yes	40.7
36	0313693	-0.79	4.0	1.11	Yes	Yes	Yes	40.8
37	0313694	-1.58	3.8	1.03	Yes	Yes	Yes	40.8
38	0314691	-2.36	3.0	0.74	Yes	Yes	No	40.4
39	0314692	-3.15	3.2	0.80	Yes	Yes	No	50.1
40	0314693	-3.94	4.0	0.93	Yes	Yes	No	48.0
41	0317691	2.00	-	0.90	Yes	Yes	No	40.7

Table 2

DIAMETER OF EXPANDED CAVITY VERSUS CHARGE DEPTH

Shot No.	d Depth (in.)	D_{max} (in.)	Shot No.	d Depth (in.)	D_{max} (in.)
40	3.94	0	29	0.20	4.53 ?
39	3.15	0	28	0.29	4.77 N
38	2.36	0	27	0.39	4.23 N
37	1.58	0	26	0.79	3.45 Y
36	0.79	0	4	1.00	4.12 Y
35	0.39	1.45 Y	10	1.00	4.15 Y
34	0.39	1.63 Y	11	1.00	No Film
33	0.20	1.46 Y	3	1.50	Early Shot
12	0	3.37 N	5	1.50	Early Shot
21	0	3.37 N	6	1.50	3.73 Y
32	0	3.19 N	23	1.97	4.37 Y
13	0.04	3.42 N	24	1.97	Early Shot
14	0.05	3.49 N	25	1.97	4.28 Y
15	0.06	No Film	2	2.00	3.99 Y
16	0.06	3.55 N	7	2.00	No Film
17	0.09	3.80 N	8	2.00	3.82 Y
18	0.09	4.21 N	41	2.00	4.42 Y
19	0.09	4.07 N	9	2.35	4.53 Y
30	0.10	4.11 N	1	2.50	No Film
20	0.10	4.20 N	22	3.44	4.07 Y
			31	3.94	4.13 Y

(?) Unknown if maximum
N Is not maximum
Y Is maximum
W = 0.038 gm
R_o = 0.072 in.

35-mm film
1-μsec exposure
40 μsec between frames

Table 3

PEAK PRESSURES VERSUS CHARGE DEPTH

Shot	d (in.)	P_m (psi) Measured	Extrapolated	Calculated Eq.(2)	Gage Depth (in.)
13	0.04	23	28	1097	1
		66	70	732	6
28	0.30	49	70	1143	1
		72	255	930	6
		15	26	309	21
10	1.00	358	550	1172	1
		194	310	711	6
9	2.35	325	410	1128	1
		219	320	837	6
31	3.94	149	320	820	1
		144	245	820	6
		18	21	320	21

Table 4

MEASURED CAVITY AND PEAK WAVE DATA

Shot Number	Charge Depth d (in.)	Cavity		Peak Wave at R = 18 in.		
		Radius R_c (in.)	Time t_c (sec)	η_m (in.)	t_m (sec)	$\frac{\eta_m R}{R_c^2}$
40	-3.94	0	none	*	*	*
39	-3.15	0	none	*	*	*
38	-2.36	0	none	*	*	*
37	-1.58	0	none	***	***	***
36	-0.79	0	none	***	***	***
35	-0.39	0.73	**	.025	3.57	.850
34	-0.39	0.82	**	.030	2.98	.802
33	-0.20	0.73	**	.015	*	.508
12	0	1.69	.006	.035	2.73	.220
21	0	1.69	**	.050	2.43	.315
32	0	1.60	.006	.030	**	.212
13	0.04	1.71	**	.030	2.60	.185
14	0.05	1.75	**	.040	3.05	.235
15	0.06	*	*	.060	2.98	*
16	0.06	1.78	.007	.060	2.27	.399
17	0.09	1.90	**	*	*	*
18	0.09	2.11	.004	.015	2.11	.061
19	0.09	2.04	**	.015	3.38	.065
30	0.10	2.06	**	.020	**	.085
20	0.10	2.10	**	**	**	**
29	0.20	2.27	**	.015	**	.052
28	0.29	2.39	.007	.025	2.28	.079
27	0.39	2.12	**	.030	**	.120
26	0.79	1.73	**	.020	**	.120
4	1.00	2.06	**	*	*	*

Continued

Table 4 (Contd)

MEASURED CAVITY AND PEAK WAVE DATA

Shot Number	Charge Depth (d) (in.)	Cavity		Peak Wave at R = 18 in.		
		Radius R_c (in.)	Time t_c (sec)	η_m (in.)	t_m (sec)	$\frac{\eta_m R}{R_c^2}$
10	1.00	2.08	.004	.030	2.00	.125
11	1.00	*	*	.045	3.09	*
3	1.50	*	*	*	*	*
5	1.50	*	*	*	*	*
6	1.50	1.87	**	.060	1.87	.309
23	1.97	2.19	**	*	*	**
24	1.97	*	*	.045	**	*
25	1.97	2.14	.004	.045	2.23	.177
2	2.00	2.00	**	*	*	*
7	2.00	*	*	.090	1.82	*
8	2.00	1.91	.003	.080	1.86	.395
41	2.00	**	**	*	*	**
9	2.35	2.27	.005	.045	2.04	.157
1	2.50	*	*	*	*	*
22	3.44	2.04	**	.035	2.15	.151
31	3.94	2.07	.004	.020	**	.083

R_o = 0.072 in.
W = 0.038 gm
d_w = 3 ft

* No data available.
** Date not reduced.
*** Data not measurable

Table 5

VALUES OF K AND T REQUIRED TO MATCH
CALCULATED AND MEASURED WAVE TRAINS

Shot Number	Charge Depth d(in.)	Cavity Radius Rc (in.)	R = Gage Range = 18	
			K	T (sec)
21	0	1.69	0.394	-0.07
16	0.06	1.78	0.408	-0.23
18	0.09	2.11	0.076	+0.01
28	0.29	2.39	0.098	+0.04
10	1.00	2.08	0.155	-0.17
25	1.97	2.14	0.222	-0.01
9	2.35	2.27	0.177	-0.13
22	3.44	2.04	0.194	-0.09

Water depth, $d_w \simeq 3$ ft.

Section 8

REFERENCES

1. Engineering-Physics Company, Hydro Shock Experiment, Final Report, Contract No. N000 14-69-C-1238, Jan 7, 1970

2. Pritchett, J. W., Explosion Product Redistribution Mechanisms for Scaled Migrating Underwater Explosion Bubbles, TR-1044, U. S. Naval Radiological Defense Laboratory, May 1966, AD 657 939

3. Kriebel, A. R., Cavities and Waves From Explosions in Shallow Water, URS 679-5, Contract N0014-67-0451, URS Research Company, Oct 1969

4. Walter, D. F., Explosion-Generated Wave Tests, Mono Lake, California, Ground and Aerial Photography, URS 654-2, Contract Nonr-4959(00), URS Research Company, Jan 1966

5. Kaplan, K., et al., A Study of Explosion-Generated Surface Water Waves, a Series of Eight Reports, URS 162-1 through 162-8, Contract Nonr-3143(00), URS Research Company, Dec 1963

6. Phillips, D. E., Analysis and Correlation of Underwater Explosion Data at NOL, Noltr-69-192, U. S. Naval Ordnance Laboratory, White Oak, Md., Dec 5, 1969

7. Phillips, D.E., and T. B. Heathcote, Underwater Explosion Tests of Two Steam Producing Explosives, I. Small Charge Tests, Noltr-66-79, U. S. Naval Ordnance Laboratory, White Oak, Md., May 23, 1966

8. Cole, R. H., Underwater Explosions, Dover Publ., N.Y., 1965

9. Snay, H. G., and A. R. Kriebel, Handbook of Underwater Nuclear Explosions, Part I - Phenomena, Chapter 5,- Shock Wave Interactions; Part II - Surface Reflection of Underwater Shock Waves, Draft for DASA 1240, URS Research Company, Dec 1969

10. Buntzen, R. R., Hydra Program, The NRDL Low-yield Underwater Explosion Tank and Associated Instrumentation, TR-623, NRDL, Feb 18, 1963, AD403022

11. Buntzen, R. R., The Use of Exploding Wires in the Study of Small-Scale Explosions, Hydra Program, TM 133, NRDL, Mar 23, 1962

12. Hege, J. W., Hydra Program, Determination of the Total Thermal Radiant Energy Emitted by an Underwater Exploding Wire, TR-612, DASA 1344, NRDL, Jan 10, 1963

13. Buntzen, R. R., The Underwater Distribution of Explosion Products From a Submerged Exploding Wire, TR-778, NRDL, July 31, 1964

14. Wallace, N. R., and C. W. Baird, Explosion-Generated Waves - 1965 Mono Lake Test Series, OSI No. 102-2, Contract Nonr 4904(00)-NR 087-159, Oceanographic Services, Inc., Dec 10, 1968

15. Hendricks, J. W., and D. L. Smith, Above-and-Below-Surface Effects of One Pound Underwater Explosions, Hydra I, TR-480, NRDL, October 1960

16. Lamb, Sir H., Hydrodynamics, 6th Ed., Dover Publ. Co., N.Y., 1932, p. 461

17. Young, G. A., The Physics of the Base Surge, Noltr 64-103, U. S. Naval Ordnance Laboratory, White Oak, Md., June 1965.

18. Brode, H. L., A Calculation of Blast Wave From a Spherical Charge of TNT, RM-1965, Rand Corp., 1957, AD 144302

19. Brode, H. L., and R. L Bjork, Cratering From a Megaton Surface Burst, RM-2600, Rand Corp., 1960, AD 250380

UNCLASSIFIED
Security Classification

DOCUMENT CONTROL DATA - R & D

(Security classification of title, body of abstract and indexing annotation must be entered when the overall report is classified)

1. ORIGINATING ACTIVITY (Corporate author)	2a. REPORT SECURITY CLASSIFICATION
URS Research Company 155 Bovet Road San Mateo, California 94402	UNCLASSIFIED
	2b. GROUP

3. REPORT TITLE

HYDRODYNAMIC DATA FROM EXPLODING WIRES

4. DESCRIPTIVE NOTES (Type of report and inclusive dates)

Annual Report

5. AUTHOR(S) (First name, middle initial, last name)

A.R. Kriebel
J.S. Bechtel

6. REPORT DATE	7a. TOTAL NO. OF PAGES	7b. NO. OF REFS
April 1, 1970	77	19

8a. CONTRACT OR GRANT NO.	9a. ORIGINATOR'S REPORT NUMBER(S)
N0014-67-C-0451	URS 679-6
b. PROJECT NO.	
c.	9b. OTHER REPORT NO(S) (Any other numbers that may be assigned this report)
d.	

10. DISTRIBUTION STATEMENT

11. SUPPLEMENTARY NOTES	12. SPONSORING MILITARY ACTIVITY
	Office of Naval Research Department of the Navy Washington, D.C. 20360

13. ABSTRACT

Hydrodynamic data are presented, and compared with previous data and theory, for a series of 41 nearly identical wires exploded between 4 in. above to 4 in. below the surface of a large volume of water under normal atmospheric pressure. The horizontal diameter of the expanded bubbles and cavities was nearly constant and equal to 4.1 in. for the submerged shots, which indicates that the equivalent yield of the exploding wires was 0.038 gm of TNT. However, the diameter decreased sharply as the wire depth approached zero closely. This indicates that the TNT equivalence dropped sharply for surface bursts, just as expected for nuclear explosions.

High-speed Schlieren photographs show nearly all of the hydrodynamic effects close to the explosions until the bubbles or cavities are fully expanded, e.g., the fireballs, cavities, bubbles, shock fronts, reflected wave fronts, and bulk cavitation. The water shock waves were measured at three locations with crystal pressure transducers, and the water surface waves were measured photographically at a horizontal range of 18 in.

The shots near the water surface generated cavities which [illegible]rly motionless and hemispherical when they became fully expanded. The water surface wave trains c[illegible]ulated from theory for such initial conditions, correspond reasonably well with those measured when empirical factors are used to allow for both a time lag and energy losses during the collapse of the cavities into turbulent breakers. Airbursts at low heights generated small hemispherical cavities.

A very distinct peak in surface wave generation was evident when the wire was exploded near the upper critical depth for the equivalent TNT charge. This is the first direct experimental evidence of the UCD effect for other than HE explosions. The expanded cavity was not abnormally large at the upper critical depth, but the plume height was apparently abnormally high. The curve for peak wave height versus depth of burst scales very well with data for TNT charges as large as 10^4 lb.

The measured peak pressures of the water shock waves were about one-third to one-half as large as predicted by equations derived empirically from data for HE and nuclear explosions with much higher yield than the wire explosions.

Additional experiments are recommended, including some scaled to nuclear tests, and some with the wire placed near the upper critical depth in shallow water and with slower cameras viewing the plume and cavity collapse. The latter experiments may show the minimum water depth required for the UCD effect, the physical cause of the effect, and its correlation with plume height and airblast.

DD FORM 1 NOV 68 1473 REPLACES DD FORM 1473, 1 JAN 64, WHICH IS OBSOLETE FOR ARMY USE.

UNCLASSIFIED
Security Classification